Daniel Correia de Matos

Licenciatura em Engenharia de Micro e Nanotecnologia

Digital Microfluidics on Paper

Dissertação para obtenção do Grau de Mestre em
Engenharia de Micro e Nanotecnologias

Orientador: Doutor Rui Alberto Garção Barreira do Nascimento Igreja, Professor Auxilar, Faculdade de Ciências e Tecnologia, Universidade Nova de Lisboa

Co-orientador: Professor Doutor Luís Miguel Nunes Pereira, Professor Auxilar, Faculdade de Ciências e Tecnologia, Universidade Nova de Lisboa

Júri:

Presidente: Doutor Rodrigo Ferrão de Paiva Martins

Arguente: Doutor Abel Martin Gonzalez Oliva

Vogal: Doutor Rui Alberto Garção Barreira do Nascimento Igreja

FACULDADE DE CIÊNCIAS E TECNOLOGIA
UNIVERSIDADE NOVA DE LISBOA

Dezembro de 2014

Digital Microfluidics on Paper

À Viagem e aos que levamos sempre connosco

Agradecimentos

Esta tese não teria sido possível sem a proposta inteligente de um tema de grande potencial por parte do Professor Rui Igreja, cujo o apoio e orientação foram essenciais na organização deste trabalho e cuja paciência, sentido de método e organização foram essenciais para colmatar as minhas próprias deficiências. Queria agradecer também ao Professor Luís Pereira na qualidade co-orientador, pelos conhecimentos transmitidos acerca das propriedades do papel e ao Professor Ricardo Franco pela perspectiva transmitida acerca dos aspectos biológicos a considerar. Gostava de agradecer também à Engenheira Diana Gaspar pelas prontidão no fornecimento das amostras de papel Sappi e FS, sempre que necessário e à Engenheira Cristina Gaspar pelo abundante fornecimento de papel Lumi que cedeu a este trabalho. Um agradecimento também para a Doutora Daniela Gomes pela esforço que se reflecte nas imagens de SEM recolhidas, à Doutora Rita Branquinho pelos ensaios de profilometria de 3D e na ajuda com o microscópio óptico, à Doutora Ana Pimentel pelos ensaios de DSC e ao Engenheiro Tomás Calmeiro não só pelo seu contributo com as imagens de AFM produzidas, mas também pelo sua constante boa disposição.

Special thanks also to Doctor Pawel Wojcik for the tips and know-how transmitted about the screen printing technique and to Engineer Michał Kurczewski for his readiness to perform the peroxidase assay, the preparation of the testing solutions and his work to improve salt concentrations to improve speed.

Queria agradecer muito especialmente ao Miguel "Rambo" Soares, Gonçalo "O Tranquilo" Rodrigues, Paul "O Alemão" Grey e Vasco "O Parvo" Rodrigues pela torfíssima irmandade que se formou neste tempo e que perdurará certamente, apesar da incerteza que se avizinha nos nossos futuros, e pelo apoio e disponibilidade para discutir ideias e especialmente pelo bom humor com que aturaram as minhas idiossincrasias. Agradeço em particular ao Vasco e ao Miguel, uma vez que conjuntamente com o Professor, começámos o projecto da Microfuídica Digital neste Departamento, num esforço colectivo. Uma palavra de agradecimento também para a Paula "A Chata" Correia pelas chamadas de atenção e conselhos frequentes, ao longo deste tempo que foram importantes para não descurar determinados aspectos do trabalho. Um enorme agradecimento aos meus amigos mais antigos que me apoiaram incondicionamente durante esta jornada, à Raquel Lourenço, Lúcia Cesário, Alexandra Silva e muito particularmente, à Ana Perdigão, cuja preocupação e tentativas de motivação e chamadas de atenção foram constantes e incansáveis e cujo o valor não consigo quantificar.

Um inesgotável agradecimento à minha família, em particular, à minha mãe Alcina e padrasto Aníbal, pelo suporte, apoio e sacrifícios que fizeram para que eu tivesse esta oportunidade. Sem eles, nada disto teria sido possível.

Abstract

This thesis is one of the first reports of digital microfluidics on paper and the first in which the chip's circuit was screen printed unto the paper. The use of the screen printing technique, being a low cost and fast method for electrodes deposition, makes the all chip processing much more aligned with the low cost choice of paper as a substrate. Functioning chips were developed that were capable of working at as low as 50 V, performing all the digital microfluidics operations: movement, dispensing, merging and splitting of the droplets. Silver ink electrodes were screen printed unto paper substrates, covered by Parylene-C (through vapor deposition) as dielectric and Teflon AF 1600 (through spin coating) as hydrophobic layer. The morphology of different paper substrates, silver inks (with different annealing conditions) and Parylene deposition conditions were studied by optical microscopy, AFM, SEM and 3D profilometry. Resolution tests for the printing process and electrical characterization of the silver electrodes were also made. As a showcase of the applications potential of these chips as a biosensing device, a colorimetric peroxidase detection test was successfully done on chip, using 200 nL to 350 nL droplets dispensed from 1 μL drops.

Keywords: Digital microfluidics; screen printing; paper microfluidics, paper device

Resumo

Esta tese é um dos primeiros registos de microfluídica digital em papel e o primeiro em que os eléctrodos foram produzidos por screen printing. A utilização desta técnica, rápida e de baixo custo, torna o processamento do dispositivo mais alinhado com o substrato de baixo custo escolhido, o papel. Dispositivos funcionais foram produzidos com a capacidade de mover gotas a tensões tão baixas como 50 V e capazes de fazer todas as operações básicas da microfluídica digital: mover, dispensar, misturar e separar gotas. Eléctrodos de prata foram depositados por screen printing num substrato de papel, cobertos por Parylene-C (por deposição de vapores) como dieléctrico e Teflon AF 1600 (por spin coating) como camada hidrofóbica. A morfologia dos diferentes substratos de papel, da tinta de prata (sujeita a diferentes condições de recozimento) e o efeito da deposição de Parylene foram estudados por microscopia óptica, AFM, SEM e profilometria 3D. Foram feitos também testes de resolução do processo de impressão e os eléctrodos de prata foram caracterizados electricamente. Gotas de de volumes entre 200 nL e 350 nL foram dispensadas de reservatórios contendo gotas de 1 μL. Para demonstrar o potencial destes chips como dipositivos de biodetecção, um teste colorimétrico de peroxidase foi feito no chip.

Palavras-chave: Microfluídica digital; Screen Printing; Microfluídica em papel; Dipositivos em papel

List of Acronyms

ABTS - 2,2'-azino-bis(3-ethylbenzothiazoline-6-sulphonic acid)

AFM – Atomic Force Microscopy

DMF – Digital Microfluidics

DSC - Differential Scanning Calorimetry

EWOD – Electrowetting on dielectric

FIB – Focused Ion Beam

FS – Felix Schoeller

HT – Hot Plate

ITO – Indium Tin Oxide

PBS - Phosphate Buffered Saline

PCB – Printed Circuit Board

PET - Polyethylene terephthalate

RMS – Root Mean Square

RPM – Revolutions per minute

SEM – Scanning Electron Microscopy

VTT - *Valtion Teknillinen Tutkimuskeskus* Technical Research Centre of Finland

List of Symbols

g – gram

h - hour

Hz – hertz

I – Current

L – liter

m – meter

M – molar

min - minutes

NaCl – Sodium chloride

s – second

t – Thickness of the dielectric

V – volts

wt% – Mass percentage

Contents

List of Figures

List of Tables

1. State of the Art

Lab-on-a-chip is the ultimate goal of a testing/detection platform. It's the search for a technology that permits in-situ, low cost, quick and high efficiency control of chemical reactions required for analysis, without the need for specialized users and enabling diagnosis in remote areas or at the point-of-decision or point-of-care[1]. The concept of digital microfluidics (DMF) is a flourishing technology that pursues this goal[2,3]. In DMF, droplets are addressed and maneuvered above the plate's array of electrodes, in sequences of any combination of the four basic fluidic operations; dispensing (creating droplets from a reservoir of fluid), moving, splitting and merging[4]; that the user or a pre-programed routine define. These operations are performed by digitally controlling the voltage applied to individual electrodes which are covered with a dielectric hydrophobic layer to create a high contact angle. The contact angle is lowered when voltage is applied to the electrodes on which the drops are, in a process often referred to as electrowetting on dielectric (EWOD)[5]. The electric field generated on the electrodes interacts with the drop and the surface of the material on which the drop is, lowering the contact angle on one side of the droplet promoting the movement. The Physics of how drop move is still not completely understood, since it works on hydrophilic and hydrophobic liquids[6], having varied applications[7] in areas from chemistry[8], to biochemistry[9] and medical analysis[10,11].

However, not all of the mentioned operations are possible with a single plate structure, requiring the use of a dual plate "sandwich" structure, with an active bottom plate and a grounded top plate[12]. The choice to use dual or single plate also influences evaporation rates of the droplets, which can be a potential problem for DMF devices, since such small volumes are being used. To also cope with this, oil can be used as filler instead of air to help reduce evaporation rates and also reducing operating voltages[3]. Even when a top plate is used, the structure of the bottom plate remains unchanged (figure 1.1). It's basically an array of electrodes deposited over a substrate which can be rigid or flexible. A dielectric layer must then cover the device to prevent current flow when voltage is applied. This layer should be thin enough as to prevent the distance between the electrode and the drop on the surface of the device of being such that it leads to an excessive attenuation of the electrical field, but should be thick enough to avoid dielectric breakdown and to help level the surface of the device, to facilitate droplet movement[13]. This later point may not be a very critical issue though, since it has been shown that in DMF it is possible to make

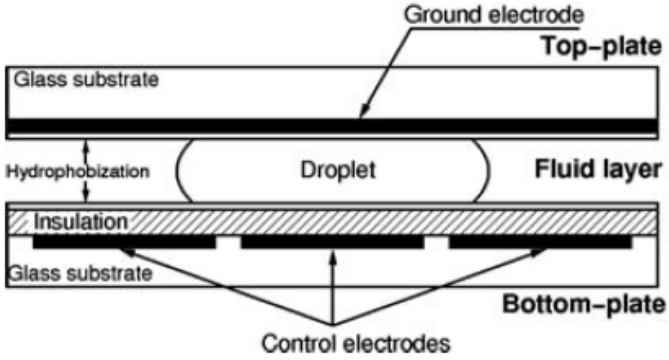

Figure 1.1 – Structure of a dual plate DMF chip.[1]

droplets move over more "adverse" surfaces[14]. On top of the dielectric layer a very thin and highly hydrophobic layer should be deposited to create a high contact angle at zero voltage. If this initial contact angle is not high enough, it'll be impossible to slide the droplet around the surface of the device, since the change in contact angle (when voltage is applied) is not enough to produce movement[13].

In terms of substrates the first choice is between the use of; rigid substrates like glass, which is compatible with typical clean-room microelectronics processes, like wet or dry etching of layers deposited by e-beam evaporation or sputtering; or flexible substrates, usually polymers (e.g. PET- Figure 1.2), which is more suitablo for non-fab and cheaper deposition/patterning methods, such as inkjet printing, screen printing and spin coating[15]. Devices using PCB technology have also been developed[16], in an attempt to adapt this already mastered technology to produce working DMF devices and try to reduce the cost when compared to other rigid substrate options. The clean room processes have the great advantage of already been mastered to a great level of process control which enable high precision in thickness and resolution definition[17]. This is not the case of inkjet printing and screen printing, where thickness control and high resolution is much more challenging[18,19]. However, pricewise, printing processes are much cheaper and thus much more compatible with low-cost, disposable devices, which are particularly interesting, especially in bioassays, to avoid contamination from the reuse of expensive devices.

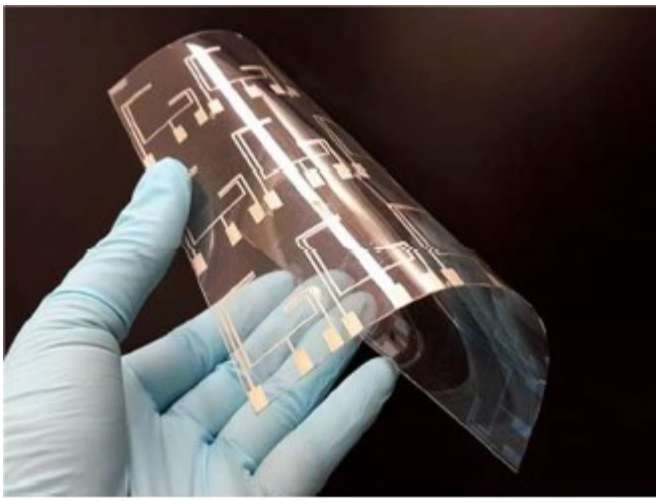

Figure 1.2 – Flexible inkjet-printed silver electrodes on a PET substrate.[15]

For the work to be developed in this thesis, the substrate chosen is paper, mainly, for two reasons: (i) it is a very low-cost material, which is a must for truly disposable devices; (ii) it can be easily disposed of[20], by incineration. This choice falls within the flexible substrate category. Also, paper based DMF devices are still a very recent concept with the first works on the subject coming out only earlier this year[21-23] and still with a lot to be explored in this new family of devices. The choice of paper as substrate means, however, that most clean-room methods are barred, since most use high temperature or high energy processes, or strong acids that can easily damage the paper. Also, clean-room processes have higher costs associated with them, which defeats the point of using a low cost substrate, since the processing costs will increase the final cost of the device.

Because of the advantages mentioned above, paper has recently gained an increasingly more prominent role in technological disposable applications as substrate and even as a functional part of

the device, being used in areas as distinct as: chemical analysis and biodetection[24], which is the case for paper microfluidics, in which paper is patterned using printed wax and where paper porosity promotes capillary force driven channels[25]; paper electronics in which the paper is both the substrate and the dielectric layer for oxide-based transistors made in a clean room environment[26,27]; and more recently an original advance has been made with the fabrication of an EWOD display on a paper substrate, in which the structure used is very similar to that of DMF, with an array of electrodes deposited on the paper, with a layer of insulating Parylene and a hydrophobic top coating of FluoroPel[14]. However, the main difference between the mentioned work and paper DMF is that in the display's case, there is a droplet over each electrode, and the intent is to apply voltage only to control the wetting of an oil layer of each water droplet to control color variation, so no droplet movement actually occurs. This has major implications in the patterning of the electrodes since they do not need to have a gap small enough as to allow the droplet to "jump" from electrode to electrode, reducing issues with process resolution. Also, to pattern the electrodes in the EWOD display's case, clean-room techniques were used, since a display is not intended to be as disposable as a biodetection fast-test platform.

The two first successful attempts at adapting a typical DMF approach to paper-based DMF devices were published only earlier this year, and both using inkjet printed electrodes, taking advantage of the added controllability. The first, by Wheeler et al[22], used silver printed on paper with an in-lab high tech inkjet printer which is very expensive but provides better resolution (achieving stable resolutions as low as 60 μm) and with operating voltages applied on the electrodes to move the drops ranging from 100 to 120 V_{rms}, driving drops with volumes from 440 nL up to 750 nL (figure 1.3). The second, by Ko et al[21], used conductive carbon nanotube electrodes printed on an adapted office printer, which is much cheaper than the in-lab one, but with a resolution over 100 μm, operating at voltages between 70 and 120 V_{rms} and moving volumes between 8 and 328 μL. However it should be taken into account the issues currently raised around the dangers of using carbon nanotubes that raise disposability issues[28,29]. Both authors produced

Figure 1.3 – Drop movement of the first published work on paper-based DMF device with inkjet printing produced electrodes.

working devices on paper, however, only the first was able to perform the whole range of microfluidic operations, as the later did not allow dispensing. Both used Parylene-C as dielectric (with thicknesses of 6.2 μm and 1 μm, respectively) deposited through vapor deposition and Teflon AF 1600 as hydrophobic layer (with thicknesses of 50 nm and 200 nm, respectively) deposited by spin coating. These first results show that although resolution might be important in lowering operating voltages, other factors, like dielectric thickness, can play a significant role as well, since the lowest operating voltage was obtained when thinner dielectric layer was used and not with the smallest separation between electrodes This clearly shows how much of an impact the optimization done can still have.

A different approach than those already tried in conventional DMF, much simpler solution, using more common materials and processes was also published earlier this year[23] and also succeeded in producing a paper-based DMF device that was able to perform two basic microfluidic operations, moving and merging drops. However, it was unable to perform splitting and dispensing. The approach presented in the referred work used spray painted graphite electrodes, patterned using a stencil, adhesive tape as dielectric and Avam rain repellant as hydrophobic layer (figure 1.4), showing other possible approaches in terms of materials and processes can be used in paper-based DMF. However, the working voltage for these devices was as high as 700 V, which is just impracticable in reality, for any kind of point-of-care application, and what is gained in the low cost of the device is then lost in the price of the control equipment that needs to produce such high voltages. This shows that the possibilities exist but there is still a lot of improving and optimization work do be done.

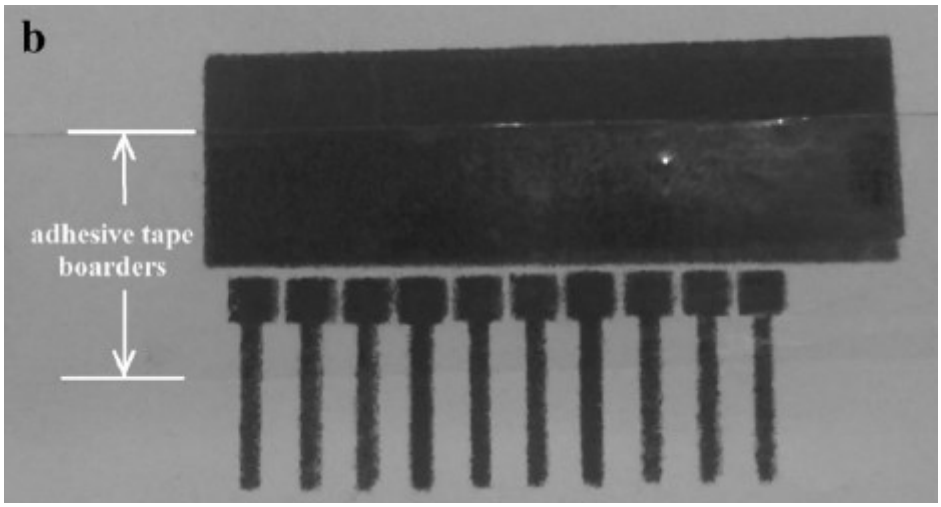

Figure 1.4 – Paper-based DMF device with spray painted graphite electrodes and adhesive tap as dielectric.

It's important to note that there is also reports of hybrid chips that combine DMF with ordinary channel microfluidics[30],creating a way of merging the advantages of channel microfluidics, with the advantages of DMF. This concept opens up also new possibilities for paper-based DMF, as similar approach could be attempted, combining the work already done with paper microfluidics in terms of detection. The DMF section of the device is able to prepare the samples that need complex

combination steps with the reagents in the form of drops, for instance, and then delivering them to microfluidic paper channel for a fast test, keeping the low cost approach.

As seen above in paper-based DMF works, in order to obtain operating voltages reasonably low and the gaps between electrodes passable, the spacing that separates them should be at the most around 100 μm, with values between 50 μm and 100 μm being preferable. These spacing are on the screen printing resolution limits, though achievable, since the mesh used, which is the thinnest model available has threads of 31 μm. Screen printing becomes then the most interesting choice for this work, since paper-based DMF devices have already been produced by inkjet printing but not with screen printing, adding a novelty value, but also because it is a simpler and cheaper process, more aligned with the idea of a low-cost device. It also is more easily scaled to large production volumes and adapted to large throutput techniques[31], which is ideal when disposable products are the aim. Since the only layer requiring patterning in DMF structure is the electrodes, it is the one that needs to be screen printed. The available materials in the lab for that purpose are carbon and silver, with silver being the most interesting choice for a first approach because of the high conductivity. To try to increase resolution and reduce the gap between electrodes, in order to reduce the operating voltage, it may be important to control the spreading of the ink after passing throught the screen, which can be modified by process parameters like speed and force applied to the squeegee but also by adjusting the properties of the ink, such as the solid content, solvent and binder quantities[32].

The following work is therefore focused on patterning the silver electrodes on a paper substrate with a manually controlled screen printing system, in an attempt to produce a paper-based device working on acceptable voltages. In order to produce a pattern that consists of adjacent features that do not contact each other, the substrate parameters must also be taken into consideration. As for the rest of the layers, the use of standard DMF procedures is the most reasonable approach, keeping the focus on the priority work and to compare it with the already existing reports. The dielectric layer used is then Parylene, particularly for the excellent conformal step coverage that it offers[33], which is even more useful when applied on high rough substrates such as paper. For this, standard vapor deposition of Parylene-C and Parylene-N could be tested, with the first yielding greater deposition rates and second yielding a better dielectric constant[34]. However, Parylene-N deposition rates are just too low for the thicknesses necessary in this work[35]. For the hydrophobic layer, typical spin coating of Teflon-AF 1600 solution is the standard, and is the most studied approach, although others can be used, like Cytop[17,36]. Characterization of the deposited layers, as to understand how each layer's characteristics might influence the final device's functioning ability is crucial, especially on morphological point of view, since it is where there is most of the unstudied characteristics so far.

2. *Materials and Methods*

2.1- Fabrication

The papers used as substrate were; LumiSilk paper, referred to as just Lumi paper, which is commercially available through Storaenso, but which was generously conceded by a partner at VTT, which recommended it for printing processes; the Sappi paper is a commercial line by the company with the same name and FS3 paper is a kind of photographic paper produced by Felix Schoeller (FS). These were chosen as they were available from other partnerships in the group working with electronic applications of paper. The silver used in the printing is SILVER PASTE LS-453-1 produced by Asahi Chemical Research Laboratory for electronics application. It was printed unto the paper using an in-lab built manual screen printing structure (figure 2.1) with a commissioned screen printing polyester monofilament mesh, model 165-31 by Maishi patterned with the desired design.

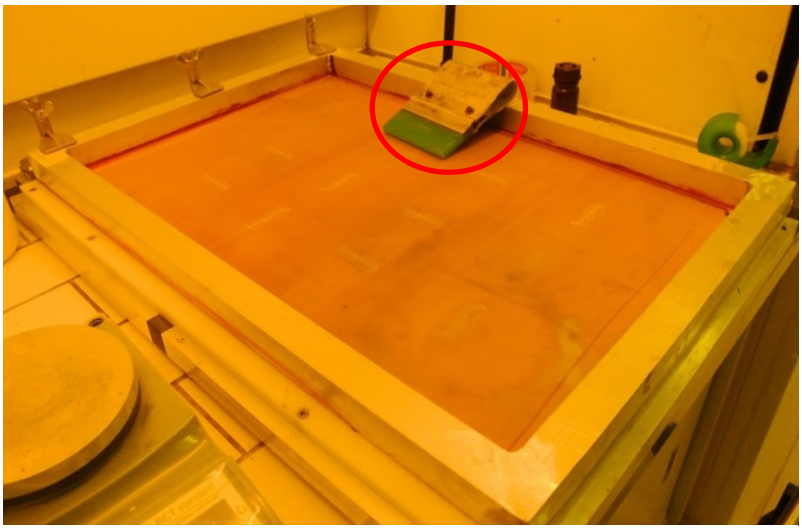

Figure 2.1 – Setup used for the screen printing process, with squeegee used to apply ink highlighted.

In the printing process, the ink was pushed through the patterns designed on the mesh using the squeegee, adjusting the printing conditions by controling the speed and force with which the blade was used to press the ink through the mesh. Annealing of the silver was done with a convection oven and hot plate in varied conditions discussed ahead.

The Parylene-C layer was applied via vapor deposition using Specialty Coating Systems - PDS 2010 LABCOATER, adjusting Parylene-C mass and process pressure to obtain the intended thicknesses. After that, the hydrophobic layer was then deposited by using a spin coating process at 1000 rpm for 30 s. A volume of 140 µL of a solution of 0.6 wt% Teflon AF 1600 on Flourinert FC-40, both by Dupont, was spun on the substrate. It was then baked on hot-plate at 150° C for 10 min, leading to a layer of about 50 nm. This Teflon coating was also applied on the top layer, which consists of ITO on glass and Teflon (which is also transparent), producing an all transparent top layer as not to block the view of the drops manipulation.

The chip design was done using Adode Ilustrator CS6 64 bit design software to produce the layout seen in figure 2.2.

This layout was done with the following considerations: first it should not have more than 8 electrodes, since the initial hardware could only cope with 8 pins;device had to be able to dispense a drop from at least two different liquids if needed, and since dispensing needs at least three electrodes in a line[12], the linear 8 electrodes configuration was selected, for simplicity purposes.

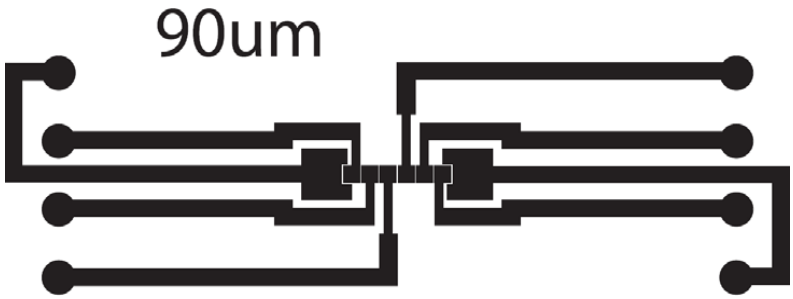

Figure 2.2 - – 90 µm example of the design used for the electrodes layout.

2.2- Controling the device

To control the device, a system like the one represented in the block diagram in figure 2.3 was used. The commands are made in the PC, communicated to a Arduino Mega unit, which multiplexes them to a high voltage switching unit, which is powered by an amplified signal. The multiplexing is what enables an individual addressing of each electrode on the DMF device, leading to electrode activation. Measurements are then made by the Arduino control board and fed back to PC.

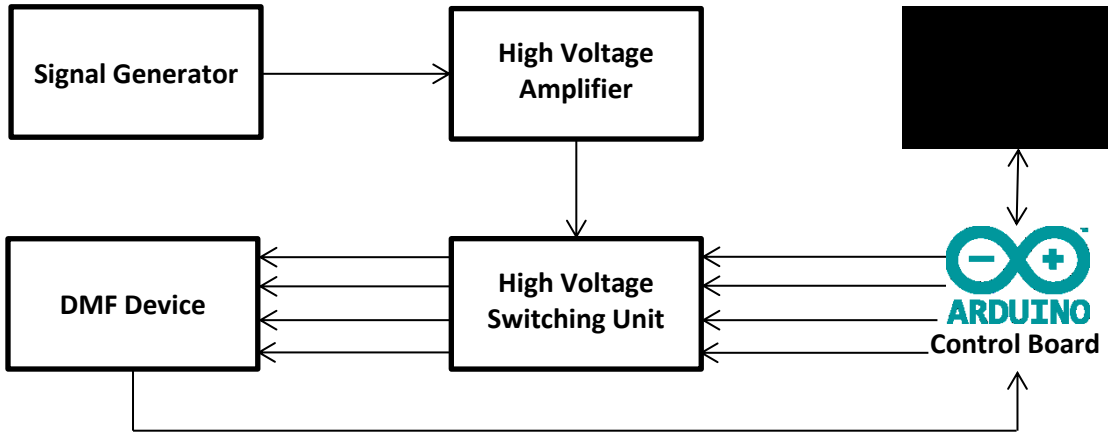

Figure 2.3 – Block Diagram of the Control System for the DMF Device

2.3- Characterization

To characterize the work that was developed several techniques were used, but focusing mostly on the morphological aspects of the layers, although not exclusively. As such an Ambios XP-Plus 200 Stylus Profilometer was used to measure the silver thickness on paper and the Parylene thickness on silicon and to perform 3D profilometry, producing topographical maps of the Lumi and Sappi papers and of the silver layer on paper. Electrodes were inspected after printing using the Olympus BX51 Optic Microscope to look for defects in the printing and measure the spacing between electrodes. Atomic Force Microscope (AFM) MFP-3D model by Asylum Research of Oxford Instruments using an Olympus AC160TS tip was used to characterize the surface topography of the paper, silver,

Parylene and Teflon at a microscale. Scanning Electron Microscopy (SEM) CrossBeam Workstation (SEM-FIB) by Zeiss Auriga was used to examine the morphology of the different papers, silver, Parylene and Teflon and was assisted with Focused Ion Beam (FIB) using a gallium liquid metal ion source to do a transversal cut of the device for examination. Contact angles were measured using a Dataphysics Contact Angle System OCA. The resistivity of the silver layers was measured using the Jandel Engineering General Purpose four point probe system.

3. *Results and Discussion*

The work that is discussed ahead is the first exploratory attempt on this subject, as DMF is a new research field, dating only more than a decade, and is a completely new subject in the department and so there was no experience in the area. Moreover, only this year the first scientific papers (2014) on paper-based DMF were published, and none of which using screen printing. As such, most of the further work is driven by the objective of producing the first working prototype of its nature, and as such, there were a lot of options that were not explored and that should be left for later work, as they were not essential for the main objective. Since the device developed is this thesis is a multilayered one, a study of each layer is necessary, to fully understand the impact of each layer's characteristics on the functionality of the final device. As such, a layer by layer approach will be conducted.

3.1- The Paper

The first component is the substrate, the paper, which has no active function in this device, serving only as physical support. Due to this, the most interesting points are its mechanical stability (in this case was not worth quantifying since the devices are not to be subjected to significant tensile strengths and are to be disposed of after one use) and the paper's surface morphology, as it will influence the morphology of the upper layers. Three different types of paper were initially considered, Lumi, Sappi and FS. Their surface, as seen on SEM, is presented for comparison purposes. Lumi is characterized by a surface covered by small crystal-like structures (with diameters under 1 μm), causing considerable roughness (Figure 3.1).

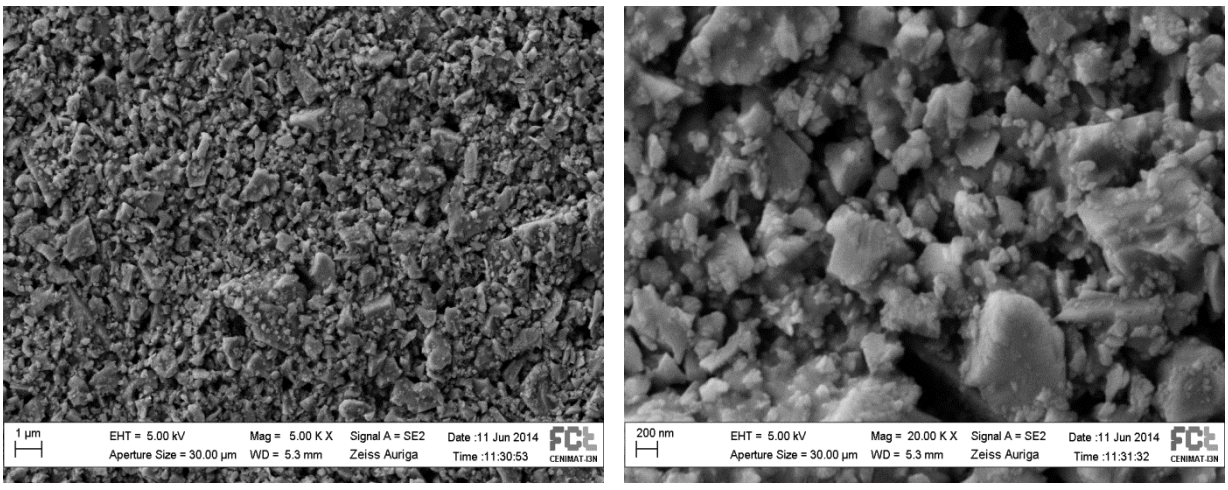

Figure 3.1 - Surface morphology of Lumi paper on SEM (Magnification: left-5k right-20k).

Next is the Sappi paper (Figure 3.2) which has two different sides, one which was treated specifically for printing processes and is the one that is supposed to be used, and another without treatment. The presented surface is from the treated side and what can be seen is the treatment's structure, which is a semi-continuous film, with some pores.

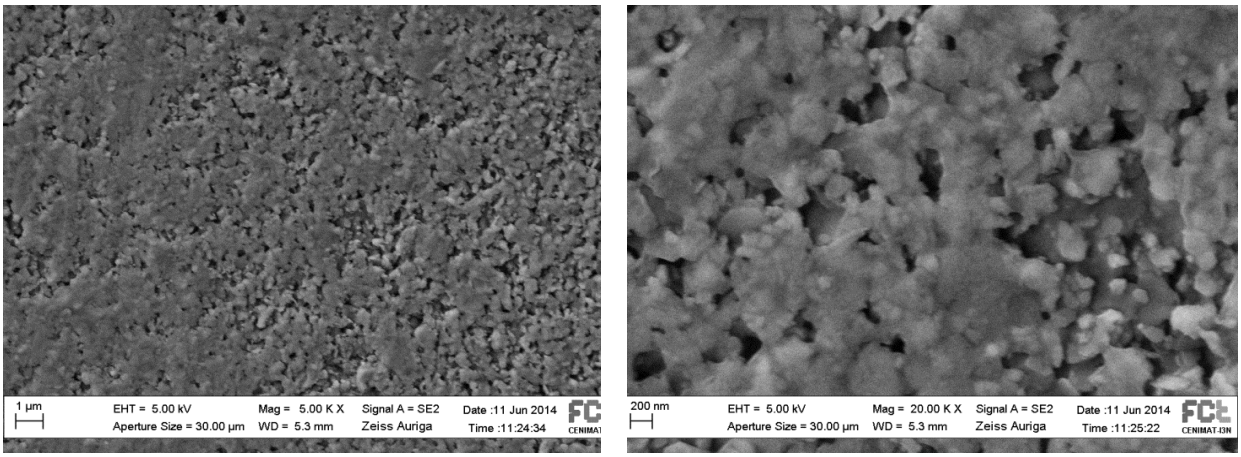

Figure 3.2 – Surface Morphology of Sappi paper on SEM (Magnification: left-5k right-20k).

The last paper tested is the FS whose surface is as seen next, the smoothest of the three kinds of papers tested (Figure 3.3). This smoothness is due to a polymeric treatment of the surface, as it resembles photographic paper. Unfortunately, no further work was pursued with this paper due to the fact that the surface treatment polymer seen here was considerably damaged by the annealing needed by the silver ink (used for the electrodes layer). This means that from the initial three types of tested paper, only two were further used.

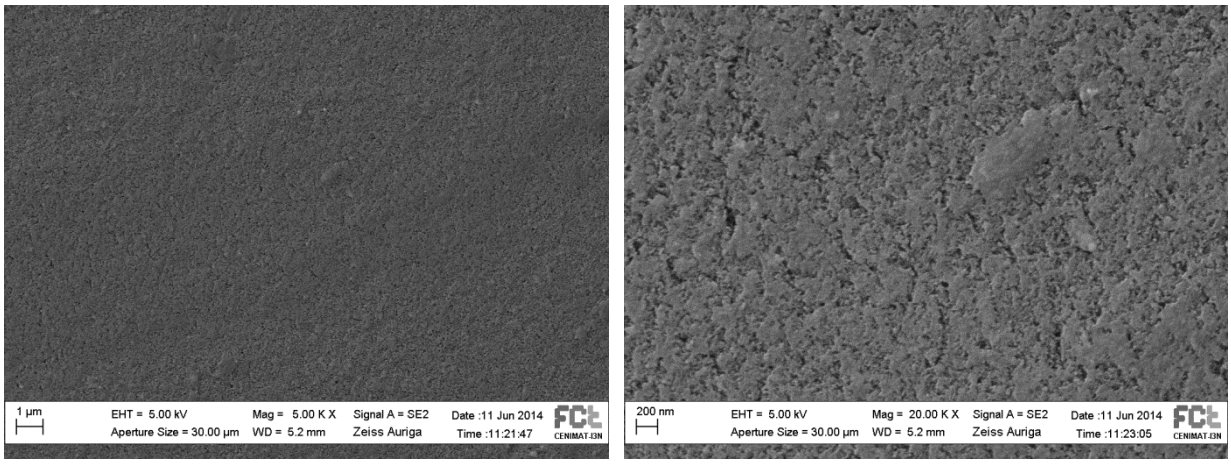

Figure 3.3 - Surface Morphology of FS paper on SEM (Magnification: left-5k right-20k).

Considering that both the Sappi and the Lumi types of paper present some surface roughness, 3D profilometry was used to quantify it in a representative scale. As such, a 1 mm by 1.4 mm area of both types of paper was scanned, producing a topographical map like the one presented in figure 3.4, which is the one for the Lumi paper and in appendix A for the Sappi paper.

For more practical comparison, the values of roughness are summarized on table 1. As can be seen, overall, there isn't a very significant difference of average or RMS roughness, with only 50 nm difference in both cases, representing only a 7% and 5% roughness variations, respectively. There a is more significant difference on the biggest peak to valley value obtained for Lumi than for Sappi, which might indicate that the features causing the roughness in the Lumi paper might be of larger

dimension than the ones in the Sappi paper, which is consistent with the SEM images shown.

Table 1 - Roughness measures obtained through 3D Profilometry

(nm)	Lumi	Sappi
Average Roughness	749	702
RMS Roughness	951	903
Peak to Valley Height	8453	6704

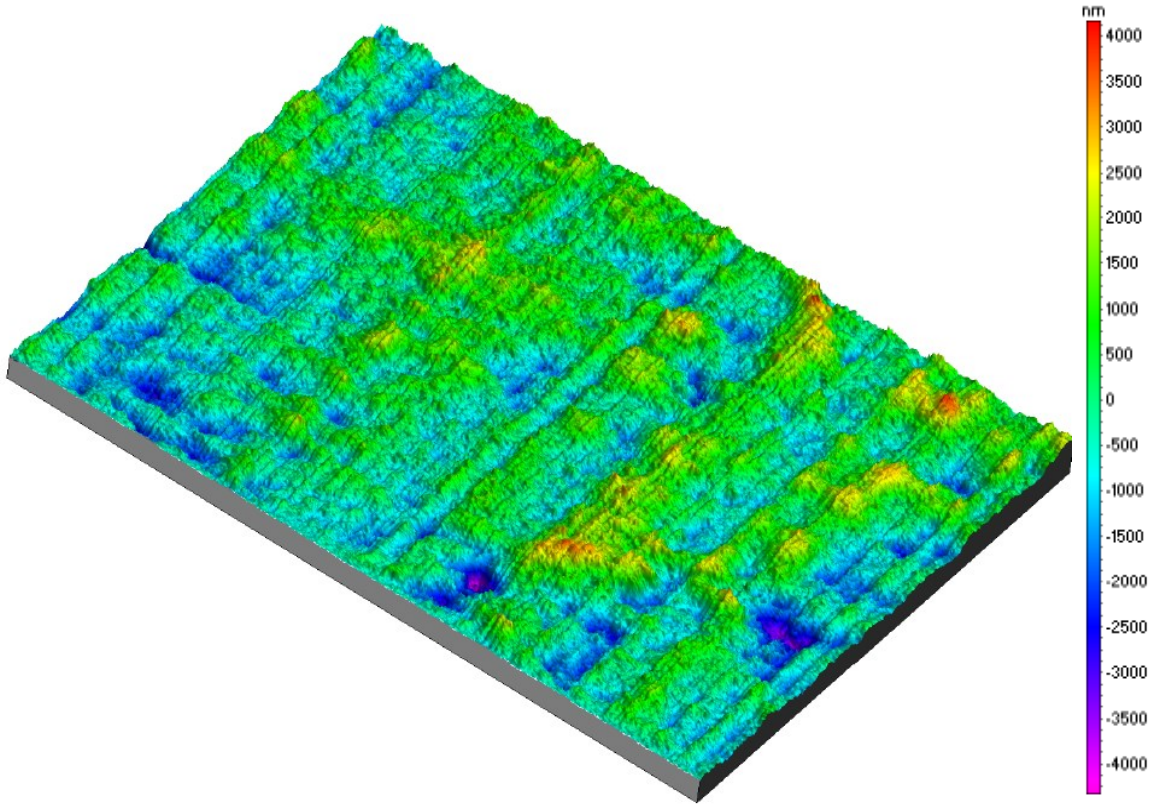

Figure 3.4 – Topographical mapping of Lumi paper through 3D profilometry on 1mm by 1.4 mm areas.

It is important to note that the dielectric properties of the paper, in certain occasions, could be somewhat relevant, although not purposely. If voltage is applied between neighboring electrodes, it could cause a parasitic capacitance. However, in normal operating conditions this should not happen, as the voltage is normally applied between the bottom and top electrodes, making the study of these properties only secondary at the most. It should be taken into account that for most of the studies done, that at first glance should not be affected by the properties of the paper (for example annealing study of the silver ink), the substrate chosen was Lumi paper, not due criteria like superior properties, but due to the abundance criteria, which should also be a factor in engineering decisions (Lumi paper was the one more available in the laboratory, as it was advised and supplied by a partner).

3.2- The Printing and the Electrodes

3.2.1 The Resolution Lines

For the printing of the actual circuit, it is fundamental to understand which is the achievable resolution, since it determines the width of the gaps between electrodes, which in turn represent the distance the drops will need to overcome to go from an electrode to another. To try to determine the actual resolution, lines like the ones shown on Figure 3.5 were produced. These are lines tens of micrometers wide and spaced by the same distance. The goal of these lines is to study what the actual final spacing obtained is after printing, when compared to the theoretical spacing.

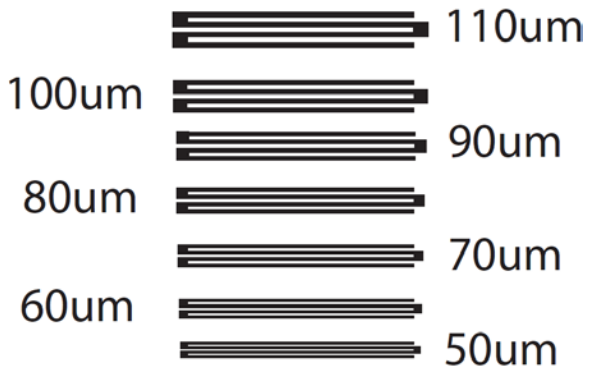

Figure 3.5 - Resolution test lines. The width of the lines is the same as the space between the lines.

The resulting patterns obtained are represented by the image on Figure 3.6a. The first thing to note is that the lines are not simple straight lines, but saw-like structures. This causes the distance between the lines to not be fixed, but to vary periodically between maximum and minimum values. This effect creates an ambiguity in the considered resolution, since that for short circuit effects, the minimum distance regions must be considered, but they do not represent the majority of the line. On

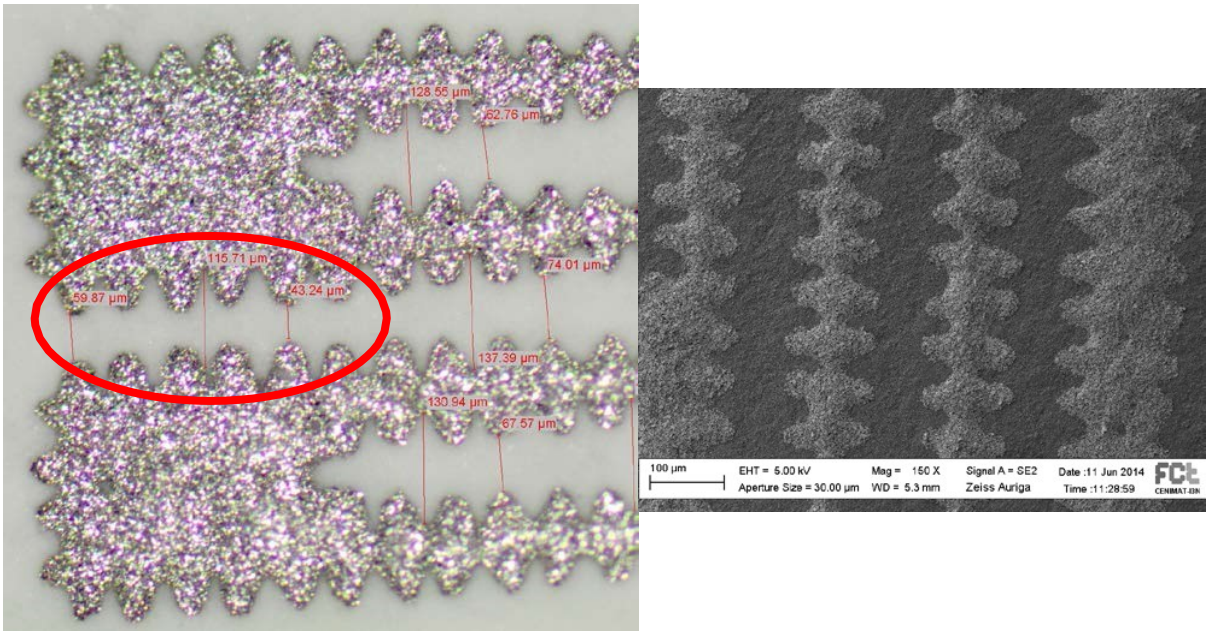

Figure 3.6 - a) (Left) Screen printed resolution lines, designed to be like seen in b) (Right) The same lines shown on SEM.

figure 3.6b it can been seen that the saw-like features are actually a chain of hill-like structures, which have a certain variable height and are connected together by valley-like features.

Throughout this analysis we should keep in mind to obtain the final pattern on paper from the

initial design on the computer, it is necessary to first pattern the mesh, using a photolitographic process, using a mask made using the initial design, and then transfer the pattern through the mesh unto the paper. So there are actually two patterning steps prior to the actual printing, the photolithographic mask patterning from the initial design, and the patterning of the mesh using the mask. So some issues in the mesh actually caused some of the patterns to be unusable, like was the case for one of the two 80 μm patterns, which had fibers crossing some electrodes (Appendix B).

Also, analyzing the values of distance obtained between the square areas at the end of lines (highlighted by the red circle in figure 13a), it is possible to see that these distances are around 20 μm smaller than the other distances between the remaining parts of the two lines. This may be because this region of the resolution lines has a bigger area than the rest of the line and this might influence ink spreading. If this is true, it will impact the final chip printing as it has features with different areas in its configuration.

3.2.2 The Device Printing

The final chip configuration has circular areas at the extremities to contact with the system on which the chip will be mounted on to operate, and as such, the length of the chip is mainly dictated by the control system. Then the conduction lines connect these outer electrodes to the actuation electrodes, which will be referred to as electrodes. These conduction lines were designed to be very wide (1 mm) for the most part, since the silver lines obtained through screen printing are less conductive than normal pure silver lines. But near the electrodes, the lines cannot be so wide or else they will distort the shape of the electrodes and will also have an active role in actuation and drop spreading, which is not intended. As such, the wideness of the lines when near the electrodes is reduced (to 0.5 mm). This way, a certain compromise between the intended drop spreading and good conductivity was achieved. As said, between the design and final printing, there is the patterning of the mesh. The overall look of a device on the mesh is in shown on Figure 3.7. It is resembles the original

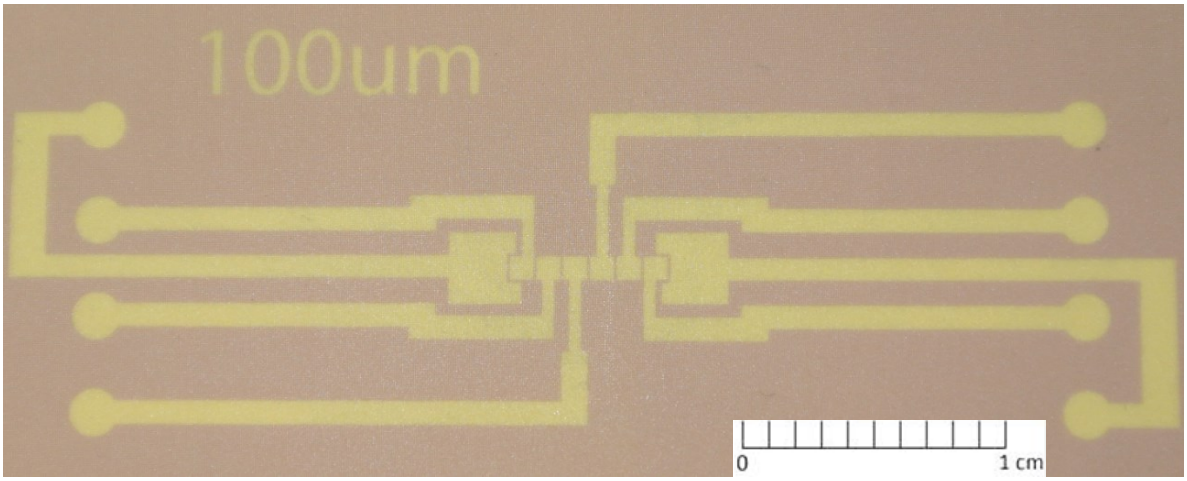

Figure 3.7 – The layout of the device on the printing mesh.

design quite closely, and it is even possible to see the spacing between electrodes. It is however, important to note that the slightly pixelated look of the picture is not only due to a pixilation on the photograph, which was taken with a very high quality camera, but primarily due to the woven fiber

matrix structure of the mesh[32].

There are two different kinds of actuation electrodes, the larger ones and the smaller ones. Both have overall square shapes, although the larger ones, called reservoirs, have a small indentation on the side to fit the other electrodes. This indentation is related to the reservoirs function on the circuit, which is to accommodate the larger drops, from which the smaller drops are dispensed. This indentation makes it easier for the smaller electrodes' pull to be felt by the larger drop and thus facilitating the dispensing process[17]. Final overall look of the printed electrodes is shown in Figure 3.8.

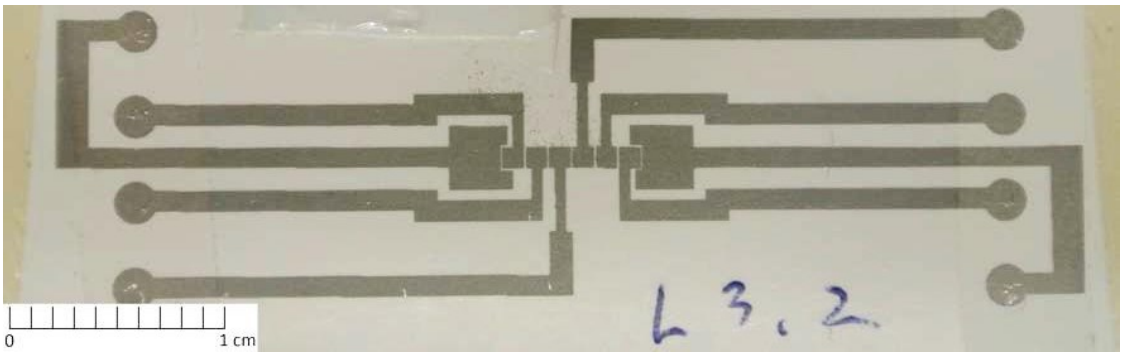

Figure 3.8 – Printed device on Lumi paper.

As said before, the spacing between neighboring electrodes is a critical factor of the process and is where the resolution is truly important. But the spacing actually attained between electrodes varies, depending on if any of the electrodes is a reservoir or not. On image 3.9, the designed spacing between

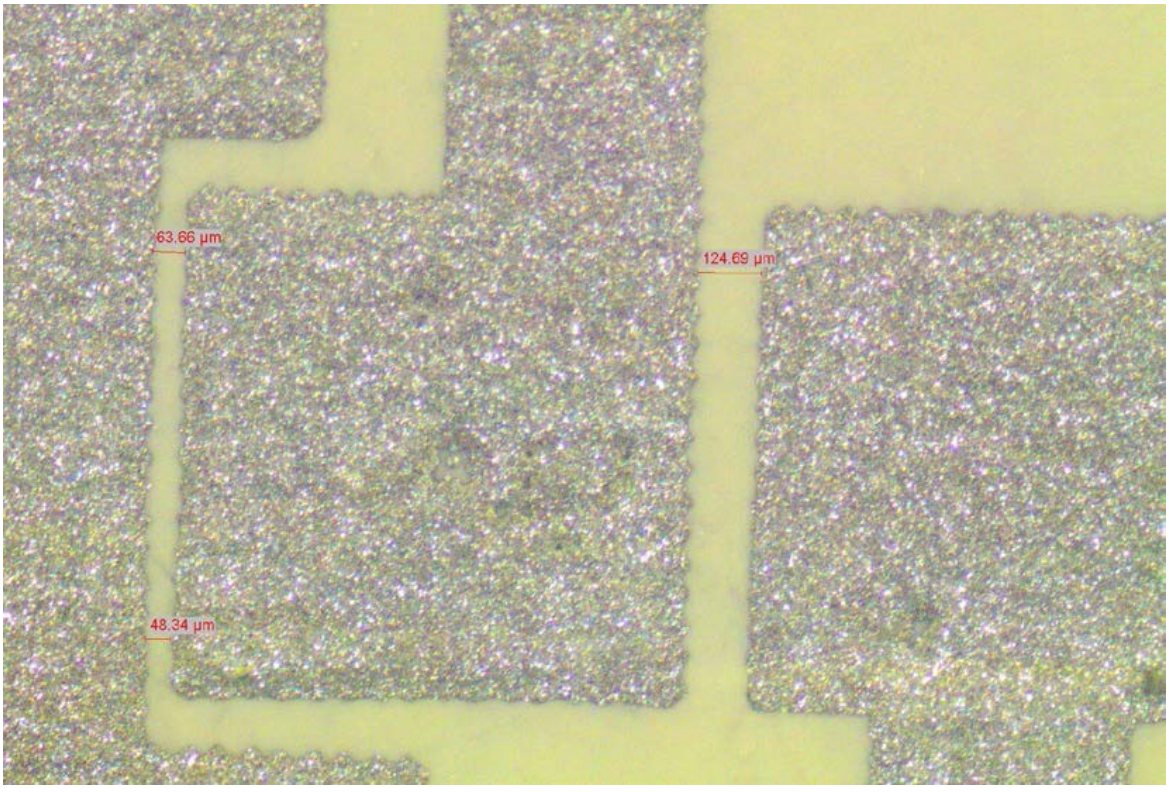

Figure 3.9 – Part of a screen printed circuit, magnified near the reservoir area.

electrodes was 90 µm. The first thing to note here is that neither the distance between two normal electrodes nor the distance between the reservoir and the neighboring electrode are actually 90 µm, the

first being larger (around 120 µm) and the second being smaller (around 50 µm).

These results were consistently found in many of the printed electrodes and the resolution lines test had already shown that neighboring larger areas registered smaller spacing. This pattern indicates bigger ink spreads on these regions since when the printing is done a certain volume of ink is transferred from the mesh to the paper. This volume depends on the height of ink, which in turn depends on the printing conditions, as the speed and force of the printing, but also depends on the area of the feature that is to be printed. If the height is such that the ink needs to spread beyond the initially intended area then, the bigger the area, the bigger the spread. The spacing variations created by this ink spread were found consistently in the printing of differently spaced devices, and actually caused frequent short-circuits between the reservoirs and neighboring circuits on the 80 µm spacing devices (appendix C). It was found then that the 90 µm spacing devices were the ones that provided the smallest possible spacing (lowering the most the operating voltage for the devices), while avoiding more frequently the short-circuit in this area (although it still happened in very high thickness printings), and so, most of the devices were printed using this spacing.

Despite the inconvenience brought, some spread is essential to the printing process, otherwise the metal lines would not be conductive, since the mesh is basically a matrix with holes through which the ink is transferred to the paper, in which each hole creates a "point" of silver. If the spread is not big enough, because the volume of ink is too small, then the points are not connected, creating a non-continuous structure, as seen figure 3.10. The mentioned figure is an example of what happens to the silver layer, when the printing process results in a low thickness deposition, with low ink spreading. This is due to a combination of strong force and high speed in the deposition motion, with a quick release, that causes a low accumulation of ink in the holes. This image makes the direct effect of the mesh's matrix-like structure on the printing process observable. The mesh's holes are 31 µm in

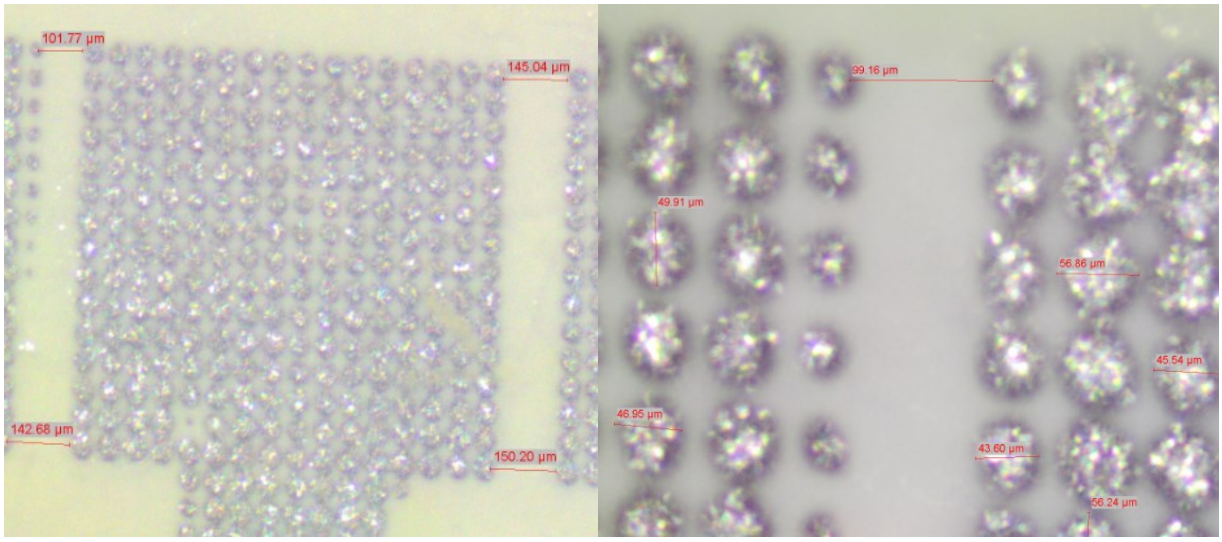

Figure 3.10 - Optical microscope image of low thickness silver. Magnification: Left 50 X; Right 100 X.

diameter while the diameter of the observed island of silver is around 50 µm, which is consistent with the initial diameter of the holes, plus some considerable spreading of the ink, although not enough to

achieve continuity.

This matrix-like structure is responsible for the saw-like structure already observed in the resolution lines and also affects the morphology of normal thickness silver layers (with thickness between 3.8 and 6.7 μm), resulting in thickness variations with a certain periodicity in the silver's structure that can be observed in the 3D profilometry of a silver large area square feature (figure 3.11). This 3D profilometry also allowed the determination of the roughness. These values can then be compared with those already obtained for the Lumi paper resulting in table 2. Comparing the obtained values and 3D topographical maps, it is possible to see that even a continuous silver layer increases significantly the surface's roughness, dominating the overall surface roughness.

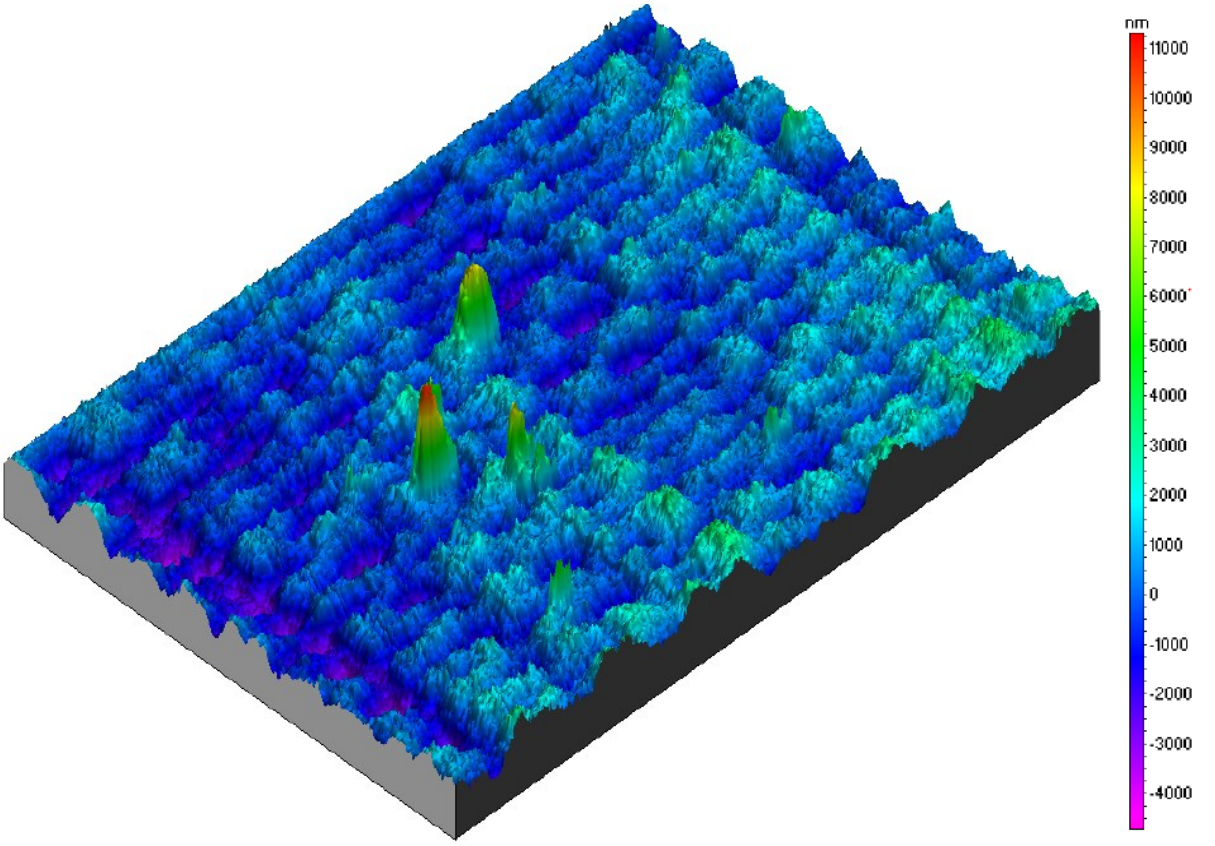

Figure 3.11 — Surface roughness 3D profile of silver film screen printed on Lumi paper and annealed on hot plate at 150 °C for 30 min. A certain periodicity can be noted.

Table 2- Comparison between the paper's original roughness and after silver deposition.

(nm)	Lumi	Silver
Average Roughness	749	930
RMS Roughness	951	1227
Peak to Valley Height	8453	16026

3.2.3 The Microstructure

The increase in roughness that is observed is not only due to the overall mountain chain structure of the silver layer, but also due to the microstructure that the silver presents. Through SEM and AFM it is possible to observe that the deposited silver actually forms a layer of overlapping flakes (Figure 3.12). In turn, these flakes seem to be constituted by aggregated silver particles. This morphology also contributes to the increase in roughness that is seen when the silver layer is deposited. This is particularly relevant if we consider that more layers will have to be deposited on top of this one (dielectric and hydrophobic layers), especially considering that heterogeneities in the dielectric layer that will be deposited directly on top of this layer may lead to dielectric breakdown, do to non- homogeneous electric fields.

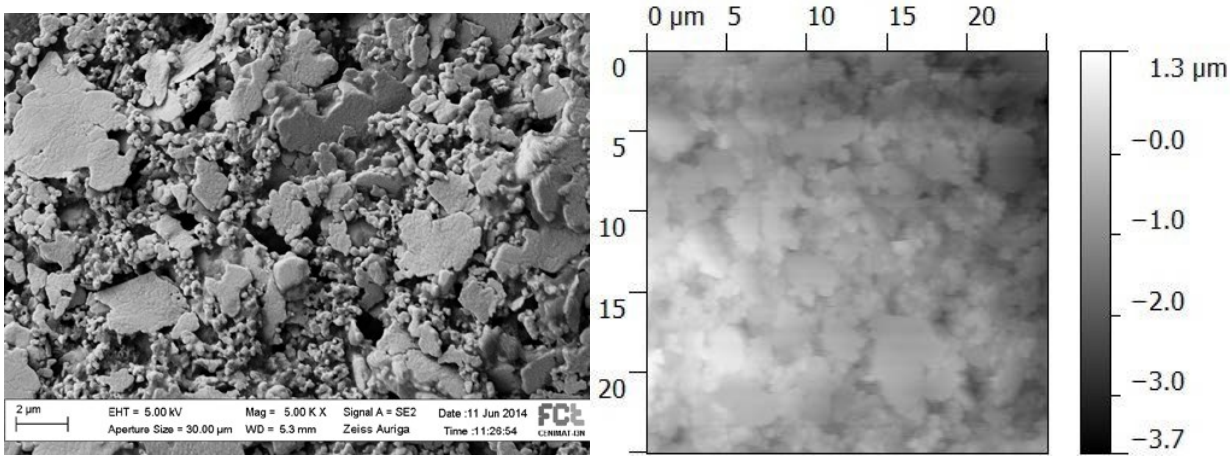

Figure 3.12 - – Microstructure of the silver film. On the left: On SEM; On the right; On AFM.

3.2.4 The Annealing

Since an annealing step is required after the printing of the silver, and since this printing was such a core challenge in the overall process, it was considered relevant to try to optimize this step, both in effectiveness and time consumption. This was particularly relevant mainly due to the fact that it was important to reach a compromise between having enough annealing temperature/time (enabling the silver layer to present high conduction and appropriated morphology characteristics), but not too much temperature/time as not to damage the paper. As such, the first approach was to characterize the stability of the paper upon temperature. Differential Scanning Calorimetry (DSC) was performed on paper, to serve as a baseline and on non-annealed silver deposited on paper, to search for signs of alterations on the silver layer that could indicate some transformation that could be associated to the annealing effect. This attempt didn't provide relevant information (the obtained graphs are in appendix D), since there are no measurably significant differences between the graph obtained for the paper alone and the one obtained for paper with silver, in the temperature range of interest (up to 300°), before the paper suffers degradation.

Considering the inconclusiveness of the DSC, another approach was attempted, that considered the effect of the annealing step on the electrical resistivity of the silver layer. Through this method,

different annealing procedures using different times and temperatures were done, and whichever produced the lowest resistivity measurement, would be our choice. Since, as seen above, thickness can vary wildly with the deposition conditions, with force and speed, and since the control of these factors is manual, to reduce human induced variability that would be introduced by big thickness variations from one sample to the next, each sample tested is actually a smaller piece cut from a big squared sample, and each piece was then subjected to its own annealing conditions. The electrical resistivity was then measured by four point probe technique and the values are presented on table 3.

Table 3 - Resistivity measurements of samples subjected to different annealing steps (HT refers to hot plate annealing, as opposed to convection oven, which is the case for the other samples.)

Applied Current 10 mA	No anneal	30 min 120°	1h 120°	30 min 150°C	1h 150°	HT 150° 10 min	HT 150° 30 min
Measured Voltage (mV)	1.00	0.17	0.16	0.17	0.14	0.21	0.17
Sheet Resistance (Ω/□)	0.45	0.08	0.07	0.08	0.06	0.10	0.08

The results for the resistivity measurements, however, are not determinant as well, even though it is curious to see that samples subjected to the same annealing time presented exactly the same values while bigger times consistently generated smaller values, the registered differences in resistivity are too small to have significant meaning other than too little time (like the 10 min on hot-plate) equals bigger resistivity. This is due to the fact the equipment used is mainly intended for more resistive films, instead of thick silver films, which result in a low voltage signal, too close to the equipment's resolution. But this is not a total setback in the sense that it means that the silver layer should be more than conductive enough for what the intended objectives. As such, another approach was used to determine the best annealing method, and that was the effect on the film morphology. To do so, samples subjected to different annealing steps were observed under SEM.

The main criteria for the choice of annealing conditions became then practicality and surface smoothness (which is relevant for device performance, as it make it easier for the Parylene-C to cover homogeneously). Looking at figure 3.13, which shows the most relevant results for the testing conditions used (the others are in appendix E), it is possible to see that the smoothness is increased by the use of the hot plate, as it seems to create a much greater surface aggregation of the flakes from which the silver layer is made of. And it does so while requiring less annealing time (30 minutes), which in turn keeps the paper whiter and less damaged, than when the convection oven (1 hour). Also in the practical sense, it is better, since with less annealing time, the process is quicker and also, it is easier to use the hot plate which heats much faster, than the oven which requires pre-heating.

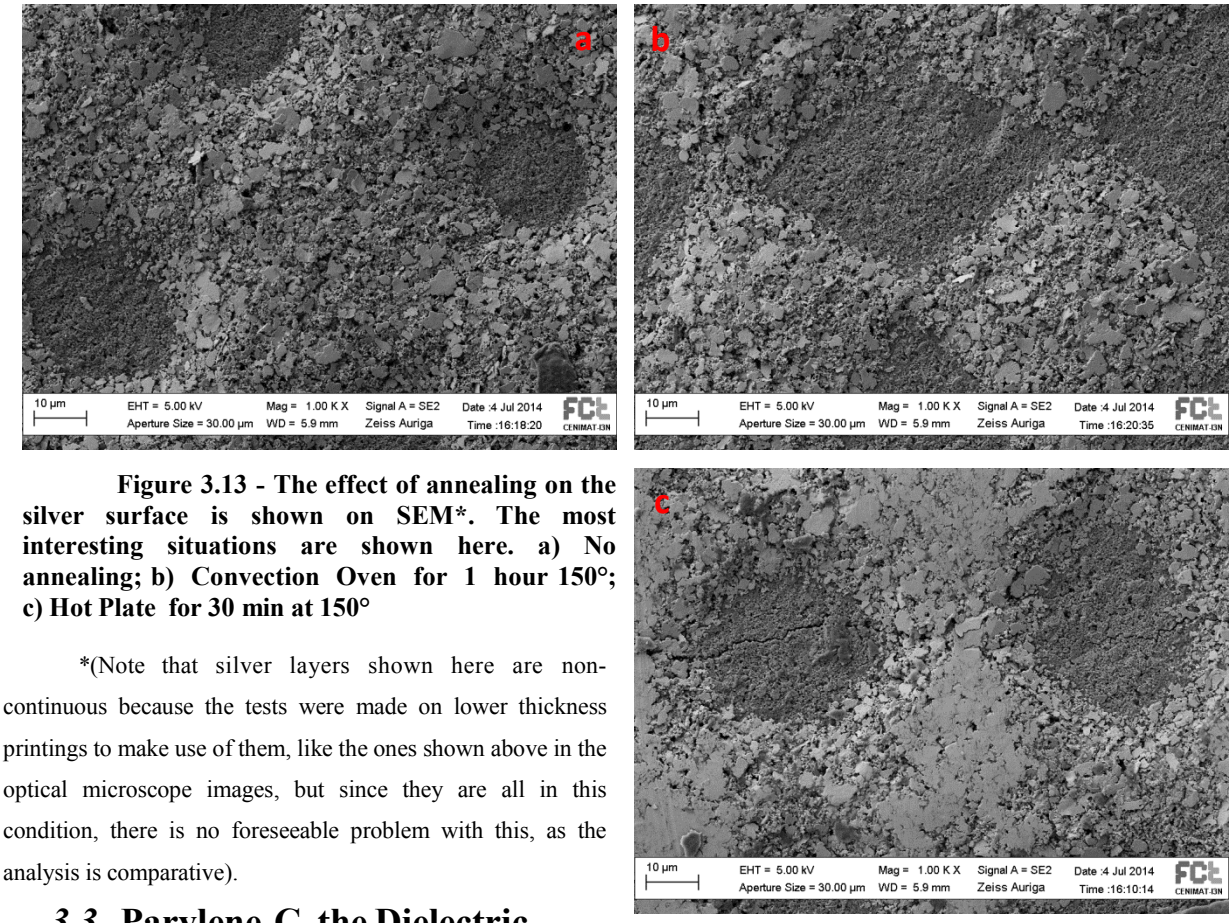

Figure 3.13 - The effect of annealing on the silver surface is shown on SEM*. The most interesting situations are shown here. a) No annealing; b) Convection Oven for 1 hour 150°; c) Hot Plate for 30 min at 150°

*(Note that silver layers shown here are non-continuous because the tests were made on lower thickness printings to make use of them, like the ones shown above in the optical microscope images, but since they are all in this condition, there is no foreseeable problem with this, as the analysis is comparative).

3.3- Parylene-C, the Dielectric

Parylene-C was initially chosen as dielectric due to a combination of favorable characteristics, as it can be deposited at room temperature through a low energy process being compatible with the use of paper substrate (when compared to sputtering) and easily reaching high thickness, which is also important as seen in the previous chapter, the spacing between electrodes can be quite high, due to resolution variability, which creates the need for higher voltages, which in turn require higher thickness, to avoid disruption. It also presents a reasonable dielectric constant value and is compatible with Teflon and its deposition process. But most of all, Parylene's deposition process has a very unique characteristic that makes it particularly suited to be the dielectric in this application which is a very good step coverage, capable of adjusting to surface morphology.

This singularity is already very interesting in normal DMF devices, as good conformal coverage of the edges of the electrodes is crucial, since it is where the electrical field becomes higher and as such, where the device is more prone to disruption. But in this paper DMF device it is even more so, since as seen above not only there is a roughness already introduced by the paper, but an even higher roughness introduced by the silver, both by the bigger mountain-like features and the microstructural flake features, which cause an overall more rugged surface to which the Parylene layer has to adjust and cover, providing a defect free dielectric layer, resistant to disruption. And exactly because of this need to avoid defects in the Parylene layer that could lead to disruption, there was a special care in the deposition conditions, which was to lower the process pressure, to values lower than those that were

usually used for the intended thicknesses. This leads to longer deposition times but more compact films, which should be free of defects. Two batches of devices were then prepared using the conditions presented on table 4.

Table 4 - Parylene deposition conditions and corresponding thicknesses measured on a flat surface (the polished side of a bit of a silicon wafer). Pressure units are specific of the equipment used.

	Mass	Pressure	Thickness (On Si)
First Batch	10 g	20	6.7 µm
Second Batch	7 g	18	4.5 µm

The first batch was made with a larger Parylene thickness to be more resistant to breakdown, even if it means higher operating voltages, as priority was set on having a working device. A second batch was made with a lower thickness but also lower process pressure, to lower operating voltage and to observe the impact in the susceptibility to breakdown. However it is very important to note that there is a certain ambiguity in what regards the final Parylene thickness obtained. Firstly because these thickness measurements were done using profilometry on silicon because the Parylene can easily be scratched by the measuring tip and when measurement is done on paper it's even more susceptible to scratching as Parylene on paper creates a rougher surface than on silicon. However it is uncertain if the thickness obtained on silicon is exactly the same as the one on paper, although is expected to be similar. But furthermore, studies performed by colleagues in the project, but whose results have not yet been published, have shown that there is some variability in the Parylene thickness depending on the relative position of the substrate in the chamber, considering both height in the chamber and distance to the center of the deposition chamber. This is to say that the thickness values obtained should be regarded as references but not as absolute values.

To observe directly the Parylene's capability to conform to surfaces, SEM images were obtained (Figure 3.14 and appendix F), showing the surface of both kinds of paper (Lumi and Sappi) before and after a 4.5 µm Parylene deposition (the images do not show exactly the same spot, but the overall morphology of the surfaces). When comparing the effect of Parylene on Lumi and Sappi paper, it is possible to observe that the surface morphology of the Parylene actually depends on the original surface morphology, confirming the conformal coverage effect of Parylene, even with a thickness as big as 4.5 µm. This can be observed in the images in figure 3.14 as the Lumi paper has larger dimension rock-like features on its surface, than the Sappi paper's smaller dimension grass-like features, and the Parylene deposited on the Lumi paper also forms larger dimension spherical features than the Parylene deposited on the Sappi paper, which also presents spherical features, but of smaller dimension.

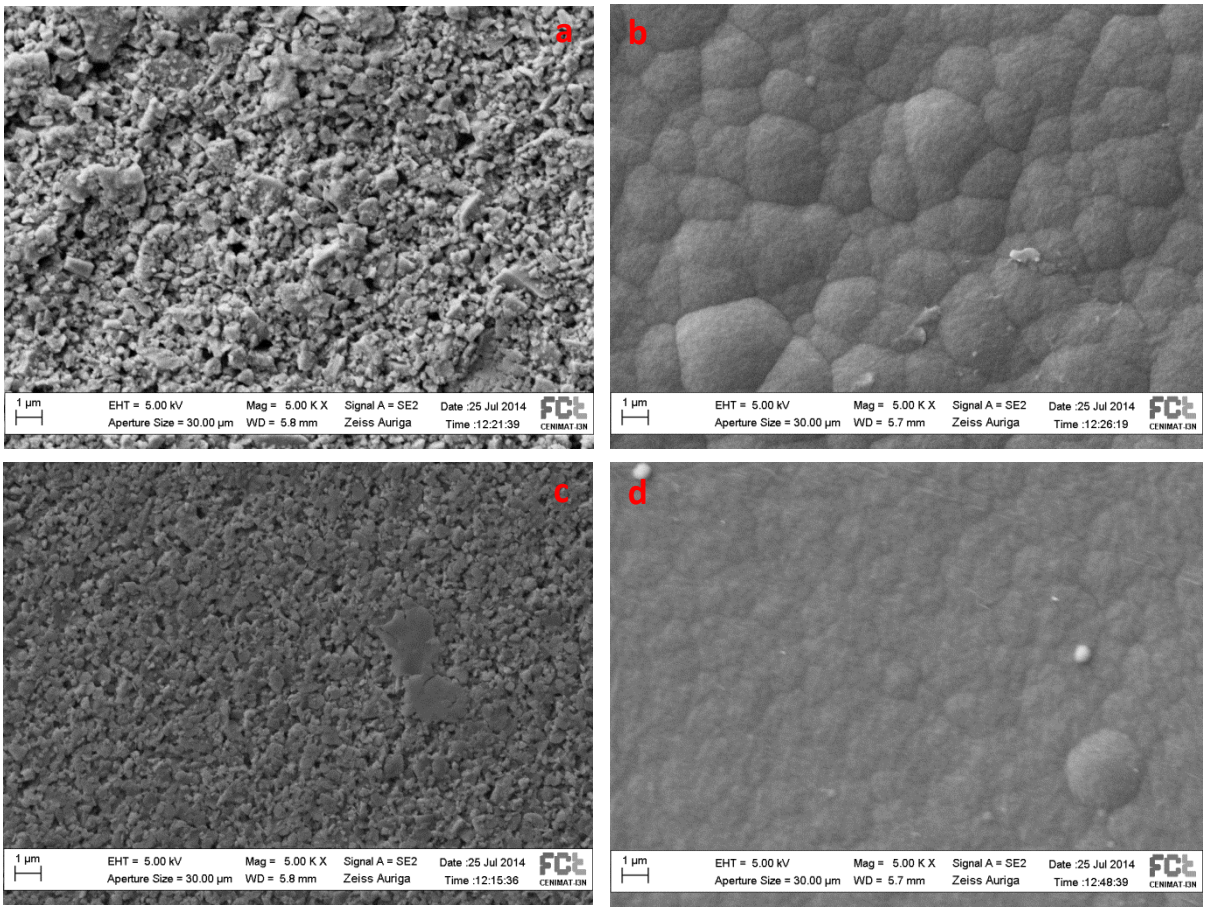

Figure 3.14 - – SEM images at same magnification. a) Lumi paper; b) Lumi paper after 4.5 µm Parylene deposition; c) Sappi paper; d) Sappi paper after 4.5 µm Parylene deposition.

However, the most of the actual working surface of the device is not composed of areas in which the Parylene is directly deposited on the paper, but of areas in which the Parylene is covering the silver electrodes, which in turn, are over the paper. Considering this, it is more relevant to look at Parylene's surface morphology when it is over the silver layer, since has been shown to adjust to the layer below. To do this, silver layers were observed also on SEM, on the same magnification as the prior images, before and after the Parylene coating. The same approach was done with silver layers deposited on both Lumi and Sappi paper, but now to study the potential effect that the papers' different surfaces could have on the final morphology of the device. The results are presented on figure 3.15 (and appendix G). The first thing to note is that the silver layers on Lumi and on Sappi have no perceivable visual differences in morphology. This result had already been predicted by 3D profilometry that showed that the silver layer is responsible for a major increase in the roughness of the surface, to values significantly higher than those of both types of paper, thus dominating surface roughness. Also, it is a result that makes sense, since the silver ink is not known to have the same conformal coverage effect that Parylene is known to have, and as such, does not follow the surface morphology of lower layers.

A direct consequence of the above is that the Parylene coating, which defines the final surface

morphology of the device, also seems to have the same surface morphology on silver regions on both kinds of paper, which does not happen on the regions without silver, example of which are the gaps between electrodes. As such, the final surface morphology of devices made on different types of paper has no differences in the active electrode regions, but is distinct in the gaps between the electrodes. So a drop when moving from one electrode to another crosses a gap with a different surface morphology than those of the electrodes. This difference of morphology depends on the type of paper. Parylene on silver seems to have a surface morphology more similar to that of Lumi paper, although the Parylene on silver seems to produce even larger dimension spherical features than those that result from the Lumi coating. So, a device made on Lumi paper has a more homogeneous surface overall, than one produced on Sappi, which will have a smoother surface between electrodes.

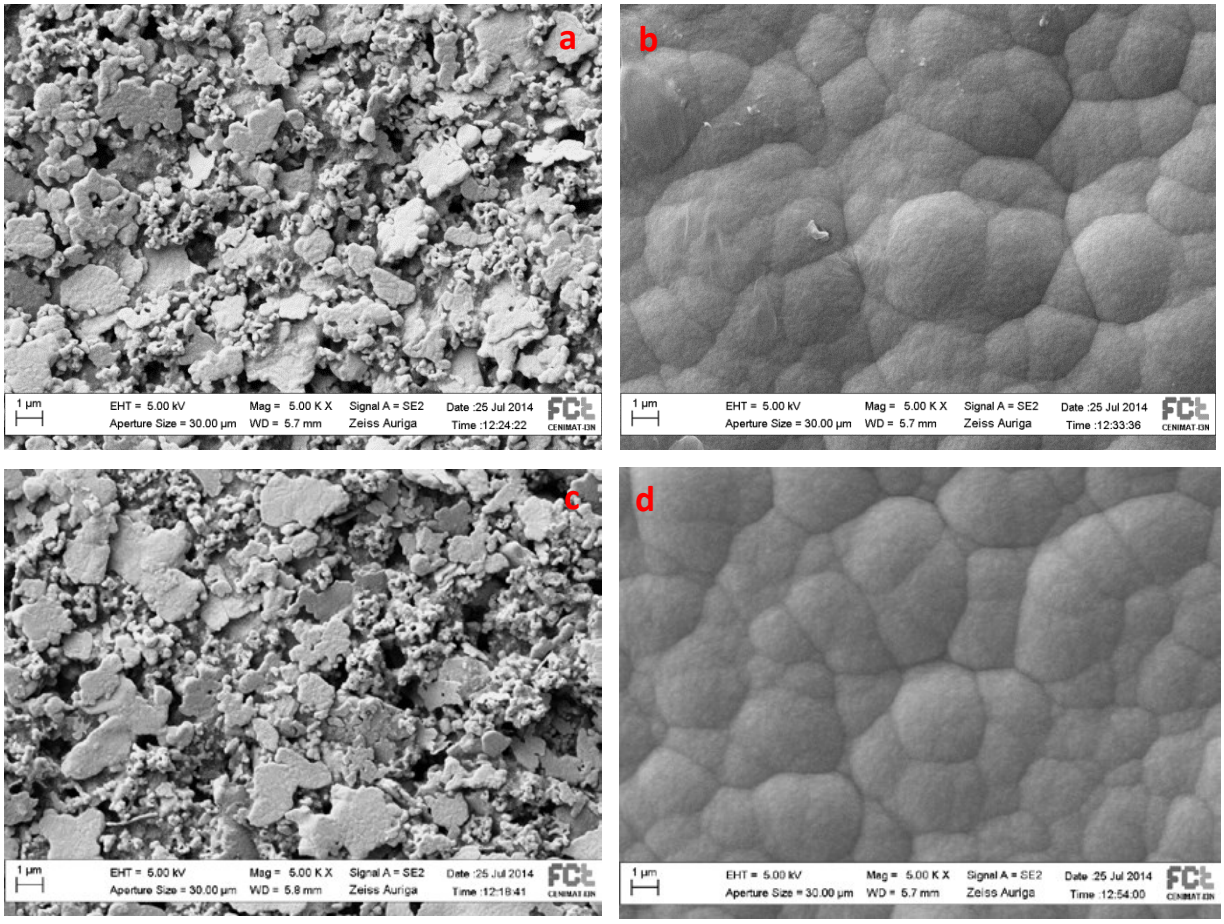

Figure 3.15 - a) Silver film on Lumi; b) Silver film on Lumi after 4.5 µm of Parylene deposition; c) Silver film on Sappi; d) Silver film on Sappi after 4.5 µm of Parylene deposition.

3.4- Teflon AF, the Hydrophobic Layer

In this thesis the superhydrophobicity inducing layer was not subjected to a study as deep as the other layers were and the option was to go with Teflon. This is due mainly to two reasons: the first of which is that the Teflon is right now a standard in DMF as the material for this layer and has already been subjected to extended studies that already predict, for instances, the deposition conditions that should be followed to reach a certain thickness and what thickness should be appropriate for this kind of application and how it should be annealed. The second reason is that at this stage the focus was

only on performance and stability. But for this kind of disposable low-cost application, cheaper solutions, even if less resilient, could be more appropriate and alternatives to Teflon should be analysed. These kind of solutions were initially considered, but it was concluded that they would be left out for further work, since this particular study will deal with polymer synthesis which was considered to be out of the scope of the present work. Still, it was considered pertinent to study how the Teflon layer adapted itself to a surface as rugged as the one presented by the Parylene on silver. As such, SEM and AFM studies were made and the AFM presented some particularly interesting results, shown on figure 3.16 and the SEM images in appendix H (the before and after Teflon images are not

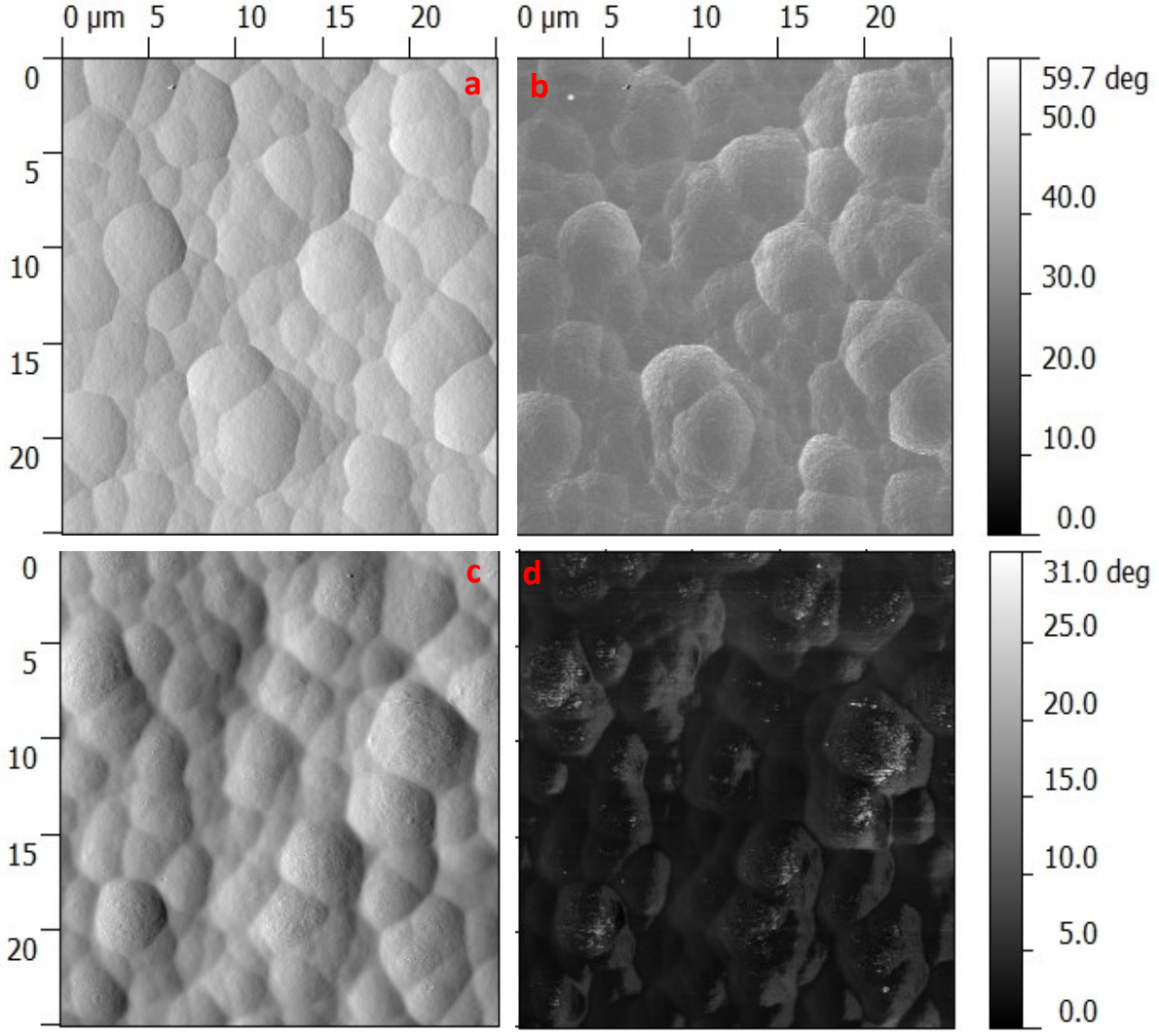

Figure 3.16 – AFM images of Parylene over silver on Lumi paper. a) and b) are before Teflon deposition, c) and d) are after. a) and c) are amplitude maps and b) and d) are phase maps.

from the same spot).

The AFM images presented testify for what is expected of the Teflon layer, when both the amplitude and the phase images are considered. Through the amplitude images, which represent the topographical aspect of the surface, it is possible to observe that the surface is not significantly modified by the Teflon layer, although some changed is noticeable, especially in the more pronounced features, where some added relief can be seen, particularly, some small particles. This is coherent with the fact that the layer deposited is very thin, only around 50 nm in thickness. But, although this layer is

very thin and causes little topographical changes, when the phase images are considered, which are more related to the specific interaction between the tip of the AFM and the surface, in terms of attractive and repulsive forces, a very significant change can be noted between the before and after Teflon images. On the after-Teflon image it can be clearly seen that some matter has been deposited on top of the sphere-like structures, creating a contrast to the lower parts. This means that the Teflon layer, on this kind of rough surface forms a non-homogeneous and maybe even not fully continuous film on the surface. Curiously, though the Teflon film may not be perfectly continuous, the overall phase image after Teflon is much darker than the before one, which in phase images means there is a more repulsive interactions between the tip and the surface. Considering that the tip is actually hydrophilic, then the increase in repulsive force in the interaction with the surface means that the surface has become more hydrophobic. So, even though the layer is not flawless, its effects are still determining the surface's hydrophobicity, as seen on contact angle measurements (Figure 3.17), in which a contact angle around 124° was obtained, which already falls on what is considered superhydrophobicity.

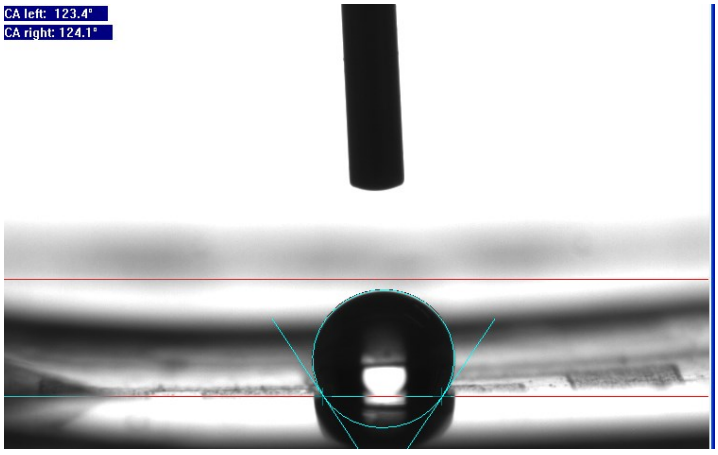

Figure 3.17 – Contact angle measurement for a 1 µl drop on a reservoir area of a fully finished device.

3.5- The Final Device

3.5.1 The final structure

To better understand how the layers of the device stacks themselves deposition process after deposition process, with particular interest on how the Parylene structures itself to conform to the silver layer and form the structures it forms, a transversal cut was made to a fully finished device using FIB and was then observed through SEM. It is important to note that to get through such a thick layer of Parylene in a reasonable time, a high current was used on the FIB, which resulted in a high power transfer, causing some melting, collapsing and peeling of the layers, which is visible on the surface (figure 3.18). Despite that, some useful information about the inner structure of the device can be obtained. There is also some material resulting from the milling process that seems to have been deposited on the surface of the device, which is normal in this kind of process and should be

disregarded.

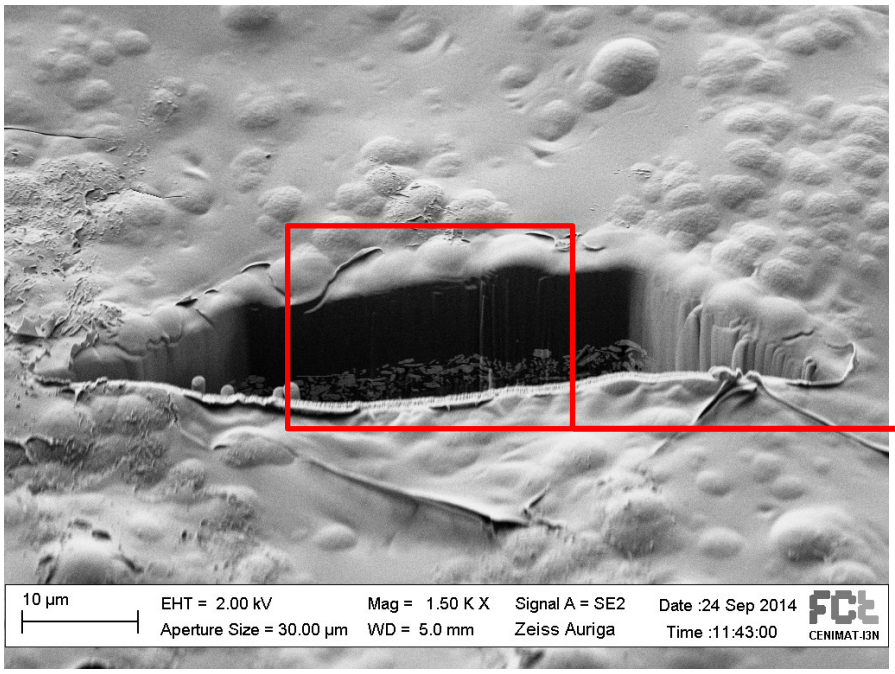

Figure 3.198 – Overall SEM image of transversal cut and of the effects on the surrounding area, of a 6.7 µm Parylene Thickness device.

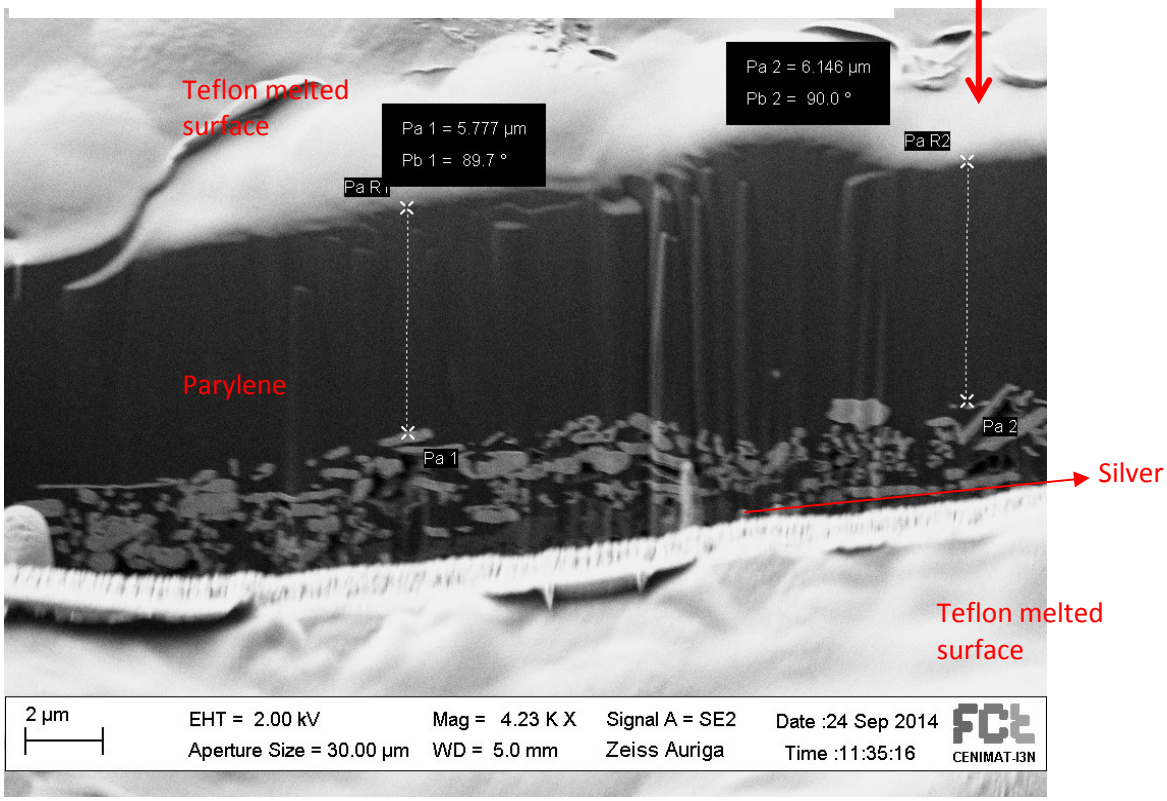

Figure 3.19 – SEM image showing further detail of the transversal cut and with Parylene thickness measurement.

The first thing to note is that it seems that the Parylene layer during its deposition process actually penetrated the surface of the silver layer, through the defects in its microstructure, already shown above, leading to some incorporation of silver in the Parylene closer to the silver layer (figure

3.19). This phenomenon can have negative effects on the device as it can lead to open circuit effects in the silver, if the Parylene is able to penetrate the whole thickness of silver and also increases the ambiguity on what's the actual Parylene thickness that should be considered for dielectric effects.

Fortunately, since the silver layer is usually several micrometers thick, the Parylene does not penetrate its entirety and as such does not seem to compromise the functioning of the device, since the particular device which was analyzed had functioned. However, the ambiguity about the Parylene thickness that should be considered as the working dielectric thickness is still increased with this incorporation of silver, and actually comes to prove that the initial decision to use a high thickness of Parylene to safeguard against disruption that could be caused by the roughness of the layers was the right decision, since a higher overall thickness reduces the effect that this mixed layer of Parylene and silver has on the devices behavior, and helps to prevent disruption.

3.6- The testing

As already said, despite the difficulties encountered in controlling the process, from the roughness induced by the several layers, in thickness control in the silver layer leading both some short-circuit and open circuit effects on the electrodes, in some cases, and uncertainty in the Parylene thickness and some homogeneity issues in the Teflon. Even with all of this several working devices were fabricated. Devices using both the 6.7 and 4.5 μm Parylene thickness were tested when mounted as seen in figure 3.20, using a triple layer of Kapton tape as spacer between the device and the top plate, creating a 150 μm height between plates do accommodate the drops. To reduce operating voltage, silicon oil was used as a medium between plates, like it is commonly done in the literature.

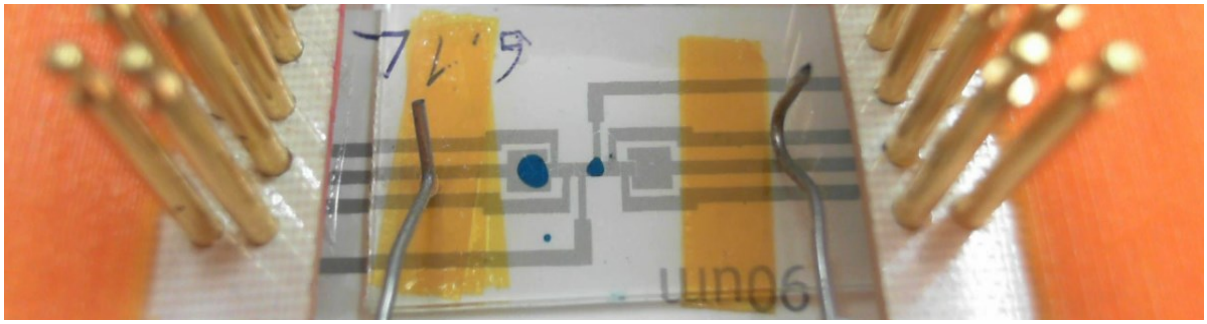

Figure 3.20 – Screen Printed DMF device mounted with top plate on control platform

The ability of the developed devices to perform the basic DMF operations was then showcased: Moving (figure 3.21), Merging (figure 3.22) and Dispensing and Splitting (figure 3.23). These images are frames of videos where the operations are performed.

Figure 3.21 - Moving drops from an electrode to another.

Figure 3.23 - Merging together two different drops.

Figure 3.22 - Dispensing a drop by splitting a smaller volume from the larger

With these operations, it is possible to sequence all the necessary steps to perform any on chip test. This is exactly what the main objective of this work intended. So the goal of producing a paper-based screen printed working device was accomplished. The volume of the drops moved is around 150 nL and they were dispensed from a 1 µL larger drop in the reservoir. The drops consisted of a 3 M solution of NaCl in deionized water. As for the operating voltages, it depended on the devices with Parylene thicknesses, with different operating voltages obtained for different thicknesses, resulting in the following table.

Table 5 – Table comprising the results of the tested conditions for which there are video records, considering testing conditions and tested devices (*only one device was produced with these conditions).

Parylene Thickness (µm)	Paper and spacing (µm)	Operating voltage (V_{rms})	Estimated average speed $mm.s^{-1}$
2*	Lumi 90	100	Breakdown
6.7	Lumi 90	100	0.125
4.5	Lumi 90	70	0.1
4.5	Lumi 80	70	0.08
4.5	Sappi 90	100	0.143

The devices with 2 μm Parylene were not mentioned before as only very few were developed under these circumstances as a test. However, they went into breakdown without moving a droplet, although EWOD was observed, (appendix I) resulting in a damaged device like the observed in appendix J. This may be better understood considering that not only a thinner dielectric in normal conditions more easily breaks down, but even more so with the silver impregnation on the Parylene layer that was seen earlier, that with thinner layers has a greater expression, reducing the breakdown voltage. As far quantitative measures are concerned, the values presented should be considered with some caution, since a low number tests per device were done and a low number of devices were tested and there is a significant variability in thickness and spreading on each device, introduced by the printing conditions. Also, speed measuring was estimated based on visual perception of the drops movement on video records, and, as such, is not the most precise, making these only overall estimated values, to give some perception of the overall situation.

Even so, it is possible to see that reducing Parylene thickness effectively reduces operating voltage, with a device with 4.5 μm Parylene on Lumi with 90 μm spacing able to move drops with only 50 V_{rms}, albeit with an impractical low speed, taking more than half a minute to move from one electrode to another. Which leads us to the next point; the speeds achieved here are significantly lower than those registered by the earlier paper-based DMF papers that used inkjet printing, which registered between 15 and 10 $mm.s^{-1}$, at their lowest. This huge reduction of speed is probably the consequence of the very rough surface morphology that has observed earlier during the characterization of the device. This roughness does not stop the drop from moving, because movement as achieved at reasonably low voltages, but it does impair the drops movement, making it much slower than it could be, by difficulting the sliding movement. The reason that there are so few registered Sappi tests is that these devices seemed to reach breakdown more easily than the Lumi-based ones, leading to more difficulties in testing. However, there is no obvious reason for this to happen, as Sappi paper is actually smoother than Lumi, and may even be just a result of a combination of random defect distribution and a smaller amount of produced devices.

3.7- The Bioassay

A final test was performed on a device, as proof of concept of the technology's potential in biodetection. The simple showcase test was a colorimetric peroxidase test and consisted on simply moving and merging two transparent drops and observing the color change produced by the reaction that occurs between the drops. The device tested was a Lumi-based 80 μm spacing chip with 6.7 μm of Parylene thickness. The 1 μL drops merged both had a NaCl concentration of 0.5M to facilitate drop movement. One drop consisted of a 0.1 mg/mL solution of horseradish peroxidase in a PBS buffer with a concentration of 10 mM and pH of 7.4. The other drop consisted of 0.05% concentration of hydrogen peroxide in an ABTS solution of 3.03 mM in a phosphate buffer with a concentration of 100 mM at a

pH of 5. When the two drops are merged, the peroxidase in the presence of peroxide degrades into water, oxidizing the ABTS, which changes from transparent into a greenish blue. The assay was done on the device, a video was made and clips are shown on figure 3.24.

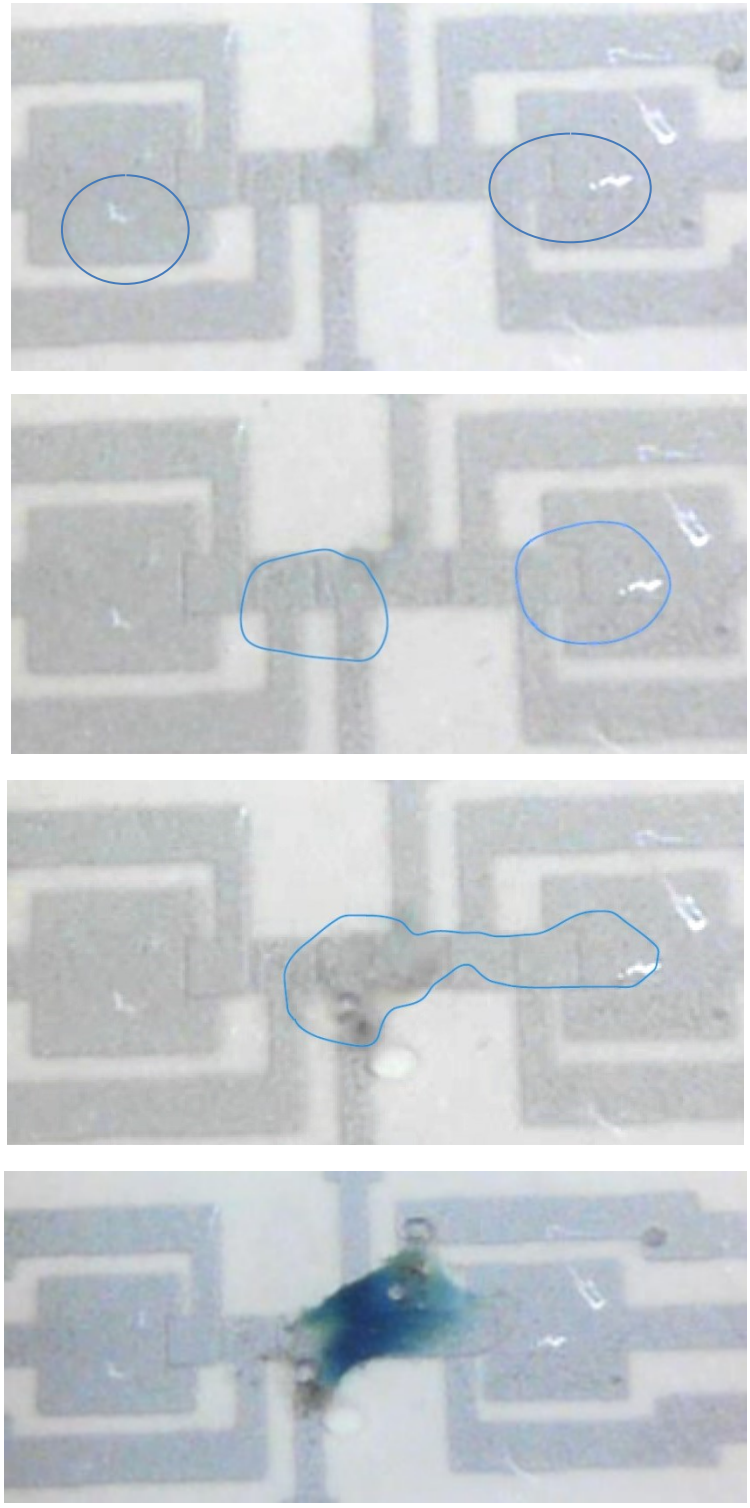

Figure 3.24 – Moving and merging of two reacting drops, promoting color change.

This final test, although simple, enough to demonstrate that this technology has indeed a potential to be explored in terms of biodetection.

4. Conclusions and Further Work

The first and foremost conclusion of this thesis is that, it is possible to produce, using a manually controlled screen printing process, working paper-based DMF devices of which, as to our knowledge, these are the first successful example. And more, not only do these devices work while being produced by a very low cost patterning process on a very low cost substrate; they are also perfectly able to perform all basic DMF operations, while resorting to reasonable, albeit not ideal, voltage values. This solution can produce very low-cost working devices, as prices associated with manual screen printed systems are very low, when compared to alternative laboratory printing solutions that had been explored so far, pushing further down the price of these kinds of devices and opening the door for other similarly functioning but bigger scale techniques to open the door to mass production, increasing accessibility and disposability, since for a device to be disposable it needs to be truly cheap. It was seen however that the process as it is currently a manual one, has its printing yield very influenced by the operator's mastery of the printing process. And even then, there is still human variability, which can still reduce the yield. But still, interestingly the devices have proved quite resilient to variability in thickness and the consequent variability in spacing between electrodes that is brought by this human factor, as long as there are no short or open-circuit defects, by being able to function, despite this variability, demonstrating a certain kind of robustness associated to the technology. However, for efficient, complex sequences of operations, higher speeds are needed than those achieved, to reduce testing time. This means that an effort should be made to reduce surface roughness of the devices, which is closely related to the surface roughness of the silver which needs smoothing. This will not only significantly increase the final device's surface smoothness due to the conformal effects of the Parylene layer and the low Teflon thickness, but will also be important to avoid Parylene incorporation in the silver, thus making it much safer to reduce Parylene thickness and further reduce operating voltages or increase droplet movement speed.

But this work is only a first approach on proving the concept of using this kind of printing technique to produce this kind of devices. Further work should be put into studying the how to control and improve the ink spreading, since it was concluded that ink spreading influences greatly the outcome of the printing process, defining resolution, thickness and playing a major part in surface of the silver, to make it smoother, as to also try to increase speed. This should lead to an optimization in the choice of the paper substrate because of the surface energy and ink absorption by the paper and also on ink formulation, to improve its viscoelastic properties. Also, other hydrophobic layers should be tested, since Teflon may be just unnecessarily expensive for what is demanded of the hydrophobic layer, and so other hydrophobic materials, like the ones used currently in textile treatments, which are much cheaper, should be explored as substitutes. In terms of the dielectric layer, further optimization into lowering and optimizing the Parylene thickness should be done, as to push further down the operating voltages, while still optimizing process pressure and other possible parameters to avoid

breakdown. Other silver inks that do not flake should also be explored or study how to avoid the flaking, as to avoid the incorporation of silver in the Parylene, as seen above, which can help reduce Parylene thickness. Finally, in regard to the printing process per se, the ultimate goal is to adapt the screen printing technique into a roll-to-toll printing technique, like flexography, so mass production is possible. As for a middle step, an adaptation to automated screen printed, with standardized printing conditions and enabling multiple depositions being printed simultaneously is the future for this kind of device, increasing yield and production rate, and reducing the current variability of both thickness and resolution.

In what applications are concerned, a very small display of the technologies capabilities was done in this thesis with the peroxidase test, leaving a lot of exploration to be done in terms of exploring all the types of tests that can be done on this platform, understanding for what kind of testing is this technology more interesting, what kind of operations should be done in what sequence and how does this all impact device layout and what kind of layout is best for each application. This is fundamental to properly tap into this technology's huge potential and is particularly critical in paper DMF, considering the fact that the lines that connect the actuation electrodes to the outer electrodes are wider to ensure good conductivity and so optimization of the design layout will be an engineering challenge for more intricate layouts. Still, this technology has a lot of potential in terms of the tests that could be done and should be explored, as it promises a great combination of accessibility, due to its low cost, flexibility, in the sequence of operations that could be done, and disposability, since it can just be burned, being adequate to test on even the most contagious of viruses. And still, the possibility of hybrid devices, combining this technology with "normal" paper microfluidics technology still remains, opening even further the scoop of possibilities to be explored with this technology.

5. Bibliography

1 Srinivasan, V., Pamula, V. K. & Fair, R. B. An integrated digital microfluidic lab-on-a-chip for clinical diagnostics on human physiological fluids. *Lab on a Chip* **4**, 310-315, doi:10.1039/b403341h (2004).

2 Fair, R. B. Digital microfluidics: is a true lab-on-a-chip possible? *Microfluidics and Nanofluidics* **3**, 245-281, doi:10.1007/s10404-007-0161-8 (2007).

3 Abdelgawad, M. & Wheeler, A. R. The Digital Revolution: A New Paradigm for Microfluidics. *Advanced Materials* **21**, 920-925, doi:10.1002/adma.200802244 (2009).

4 Cho, S. K., Fan, S. K., Moon, H. J., Kim, C. J. & Ieee. in *15th IEEE International Conference on Micro Electro Mechanical Systems (MEMS 2002).* 32-35 (Ieee, 2002).

5 Lee, J., Moon, H., Fowler, J., Schoellhammer, T. & Kim, C. J. Electrowetting and electrowetting-on-dielectric for microscale liquid handling. *Sensors and Actuators a-Physical* **95**, 259-268, doi:10.1016/s0924-4247(01)00734-8 (2002).

6 Chatterjee, D., Hetayothin, B., Wheeler, A. R., King, D. J. & Garrell, R. L. Droplet-based microfluidics with nonaqueous solvents and solutions. *Lab on a Chip* **6**, 199-206, doi:10.1039/b515566e (2006).

7 Jebrail, M. J., Bartsch, M. S. & Patel, K. D. Digital microfluidics: a versatile tool for applications in chemistry, biology and medicine. *Lab on a Chip* **12**, 2452-2463, doi:10.1039/c2lc40318h (2012).

8 Zhu, Y. & Fang, Q. Analytical detection techniques for droplet microfluidics-A review. *Analytica Chimica Acta* **787**, 24-35, doi:10.1016/j.aca.2013.04.064 (2013).

9 Teh, S.-Y., Lin, R., Hung, L.-H. & Lee, A. P. Droplet microfluidics. *Lab on a Chip* **8**, 198-220, doi:10.1039/b715524g (2008).

10 Lun, F. M. F. *et al.* Microfluidics digital PCR reveals a higher than expected fraction of fetal DNA in maternal plasma. *Clinical Chemistry* **54**, 1664-1672, doi:10.1373/clinchem.2008.111385 (2008).

11 Sista, R. *et al.* Development of a digital microfluidic platform for point of care testing. *Lab on a Chip* **8**, 2091-2104, doi:10.1039/b814922d (2008).

12 Cho, S. K., Moon, H. J. & Kim, C. J. Creating, transporting, cutting, and merging liquid droplets by electrowetting-based actuation for digital microfluidic circuits. *Journal of Microelectromechanical Systems* **12**, 70-80, doi:10.1109/jmems.2002.807467 (2003).

13 Moon, H., Cho, S. K., Garrell, R. L. & Kim, C. J. Low voltage electrowetting-on-dielectric. *Journal of Applied Physics* **92**, 4080-4087, doi:10.1063/1.1504171 (2002).

14 Kim, D. Y. & Steckl, A. J. Electrowetting on Paper for Electronic Paper Display. *Acs Applied Materials & Interfaces* **2**, 3318-3323, doi:10.1021/am100757g (2010).

15 He, F., Grimes, J., Alcaine, S. D. & Nugen, S. R. A hybrid paper and microfluidic chip with electrowetting valves and colorimetric detection. *Analyst* **139**, 3002-3008, doi:10.1039/c3an01516e (2014).

16 Gong, J. & Kim, C.-J. Direct-referencing two-dimensional-array digital microfluidics using multilayer printed circuit board. *Journal of Microelectromechanical Systems* **17**, 257-264, doi:10.1109/jmems.2007.912698 (2008).

17 Lin, Y. Y., Welch, E. R. F. & Fair, R. B. Low voltage picoliter droplet manipulation utilizing electrowetting-on-dielectric platforms. *Sensors and Actuators B-Chemical* **173**, 338-345, doi:10.1016/j.snb.2012.07.022 (2012).

18 Calvert, P. Inkjet printing for materials and devices. *Chemistry of Materials* **13**, 3299-3305, doi:10.1021/cm0101632 (2001).

19 Muller, C. D. *et al.* Multi-colour organic light-emitting displays by solution processing. *Nature* **421**, 829-833, doi:10.1038/nature01390 (2003).

20 Shitanda, I., Yamaguchi, T., Hoshi, Y. & Itagaki, M. Fully Screen-printed Paper-based Electrode Chip for Glucose Detection. *Chemistry Letters* **42**, 1369-1370, doi:10.1246/cl.130681 (2013).

21 Ko, H. *et al.* Active Digital Microfl uidic Paper Chips with Inkjet- Printed Patterned Electrodes. *Advanced Materials* **26**, 2335-2340, doi:10.1002/adma.201305014 (2014).
22 Fobel, R., Kirby, A. E., Ng, A. H. C., Farnood, R. R. & Wheeler, A. R. Paper Microfluidics Goes Digital. *Advanced Materials* **26**, 2838-2843, doi:10.1002/adma.201305168 (2014).
23 Abadian, A. & Jafarabadi-Ashtiani, S. Paper-based digital microfluidics. *Microfluidics and Nanofluidics* **16**, 989-995, doi:10.1007/s10404-014-1345-7 (2014).
24 Costa, M. N. *et al.* A low cost, safe, disposable, rapid and self-sustainable paper-based platform for diagnostic testing: lab-on-paper. *Nanotechnology* **25**, doi:10.1088/0957-4484/25/9/094006 (2014).
25 Carrilho, E., Martinez, A. W. & Whitesides, G. M. Understanding Wax Printing: A Simple Micropatterning Process for Paper-Based Microfluidics. *Analytical Chemistry* **81**, 7091-7095, doi:10.1021/ac901071p (2009).
26 Martins, R. *et al.* Write-erase and read paper memory transistor. *Applied Physics Letters* **93**, 3, doi:10.1063/1.3030873 (2008).
27 Fortunato, E. *et al.* High-performance flexible hybrid field-effect transistors based on cellulose fiber paper. *Ieee Electron Device Letters* **29**, 988-990, doi:10.1109/led.2008.2001549 (2008).
28 Klaine, S. J. *et al.* Nanomaterials in the environment: Behavior, fate, bioavailability, and effects. *Environmental Toxicology and Chemistry* **27**, 1825-1851, doi:10.1897/08-090.1 (2008).
29 Nel, A., Xia, T., Madler, L. & Li, N. Toxic potential of materials at the nanolevel. *Science* **311**, 622-627, doi:10.1126/science.1114397 (2006).
30 Abdelgawad, M., Watson, M. W. L. & Wheeler, A. R. Hybrid microfluidics: A digital-to-channel interface for in-line sample processing and chemical separations. *Lab on a Chip* **9**, 1046-1051, doi:10.1039/b820682a (2009).
31 Krebs, F. C., Tromholt, T. & Jorgensen, M. Upscaling of polymer solar cell fabrication using full roll-to-roll processing. *Nanoscale* **2**, 873-886, doi:10.1039/b9nr00430k (2010).
32 Krebs, F. C. Fabrication and processing of polymer solar cells: A review of printing and coating techniques. *Solar Energy Materials and Solar Cells* **93**, 394-412, doi:10.1016/j.solmat.2008.10.004 (2009).
33 Kahouli, A. *et al.* Structural and dielectric study of parylene C thin films. *Applied Physics Letters* **94**, 3, doi:10.1063/1.3114404 (2009).
34 Fortin, J. B. & Lu, T. M. A model for the chemical vapor deposition of poly(para-xylylene) (parylene) thin films. *Chemistry of Materials* **14**, 1945-1949, doi:10.1021/cm010454a (2002).
35 Tacito, R. D. & Steinbruchel, C. Fine-line patterning of parylene-n by reactive ion etching for application as an interlayer dielectric. *Journal of the Electrochemical Society* **143**, 1974-1977, doi:10.1149/1.1836934 (1996).
36 Li, Y. F. *et al.* Room-Temperature Fabrication of Anodic Tantalum Pentoxide for Low-Voltage Electrowetting on Dielectric (EWOD). *Journal of Microelectromechanical Systems* **17**, 1481-1488, doi:10.1109/jmems.2008.2006827 (2008).

6. Appendix

Apendix A

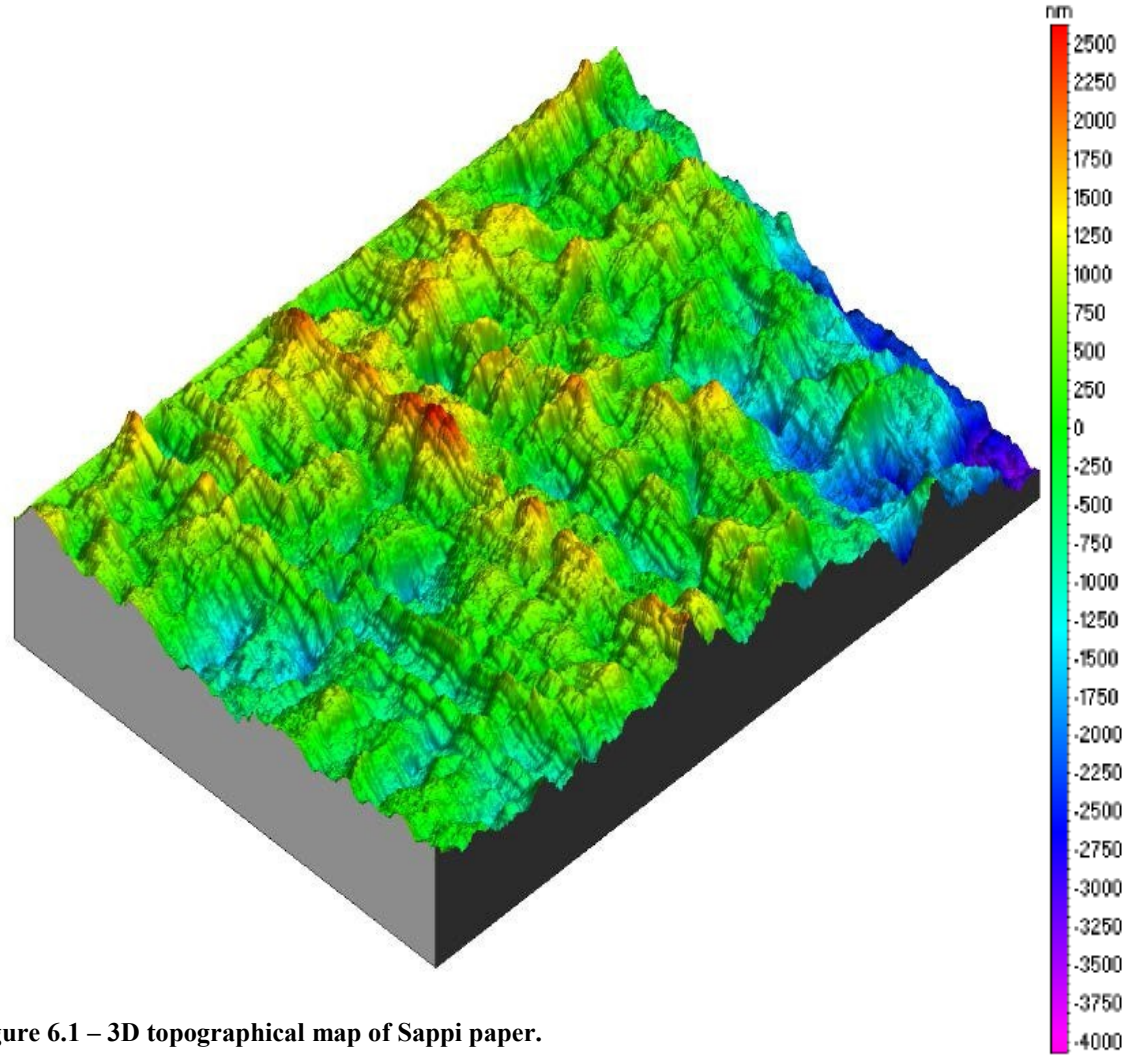

Figure 6.1 – 3D topographical map of Sappi paper.

Appendix B

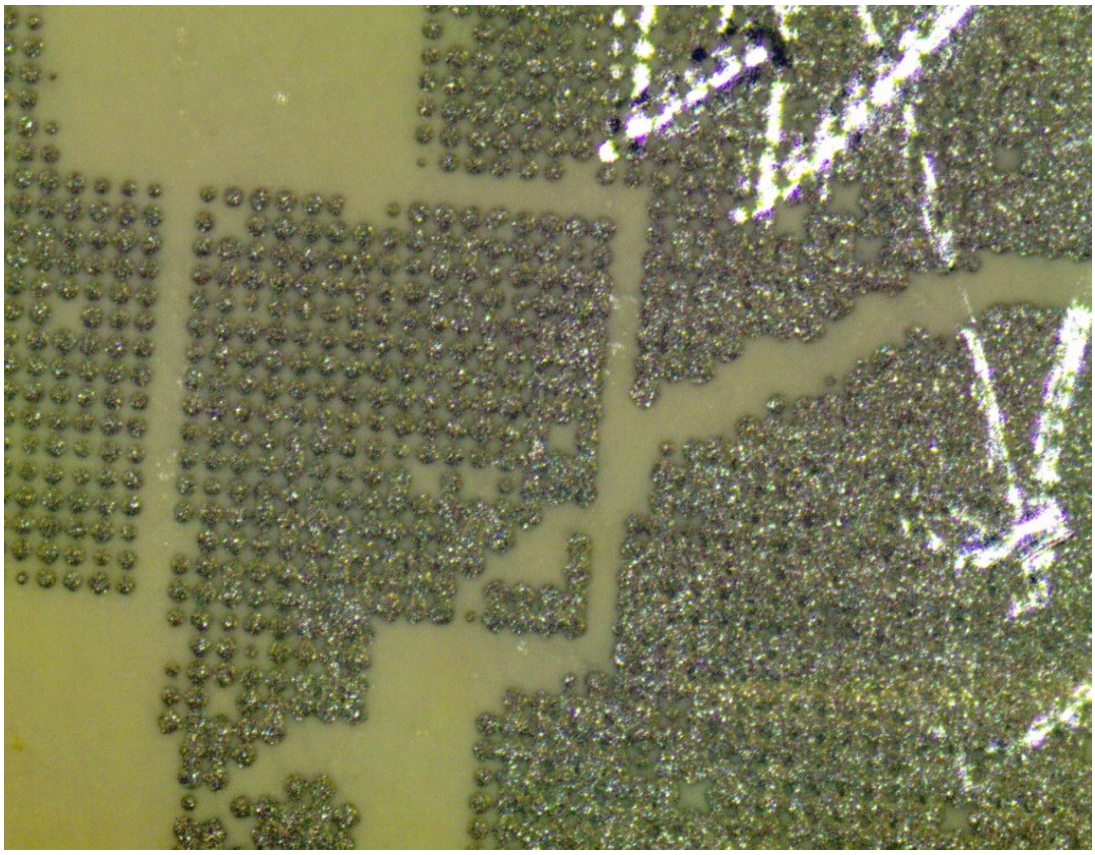

Figure 6.2 – Example of a device printed through the defective 80 µm pattern.

Appendix C

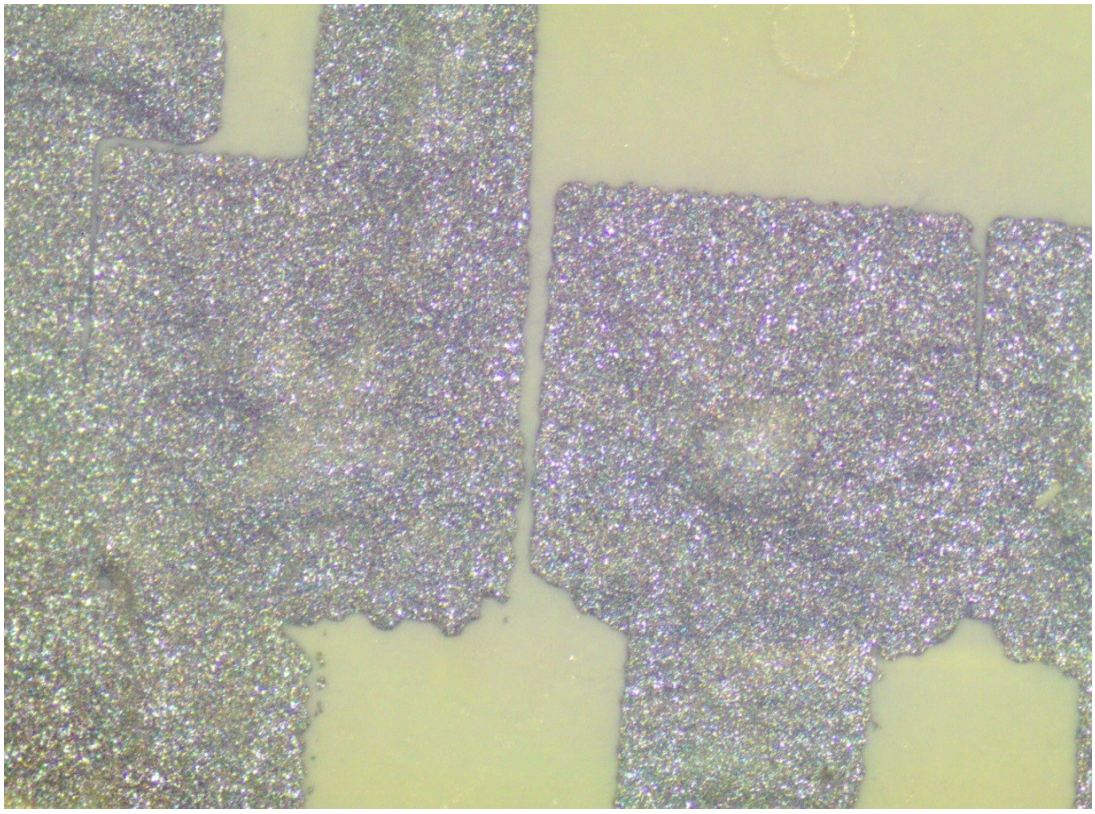

Figure 6.3 – Short circuit on the reservoir area of a 80 µm device

Appendix D

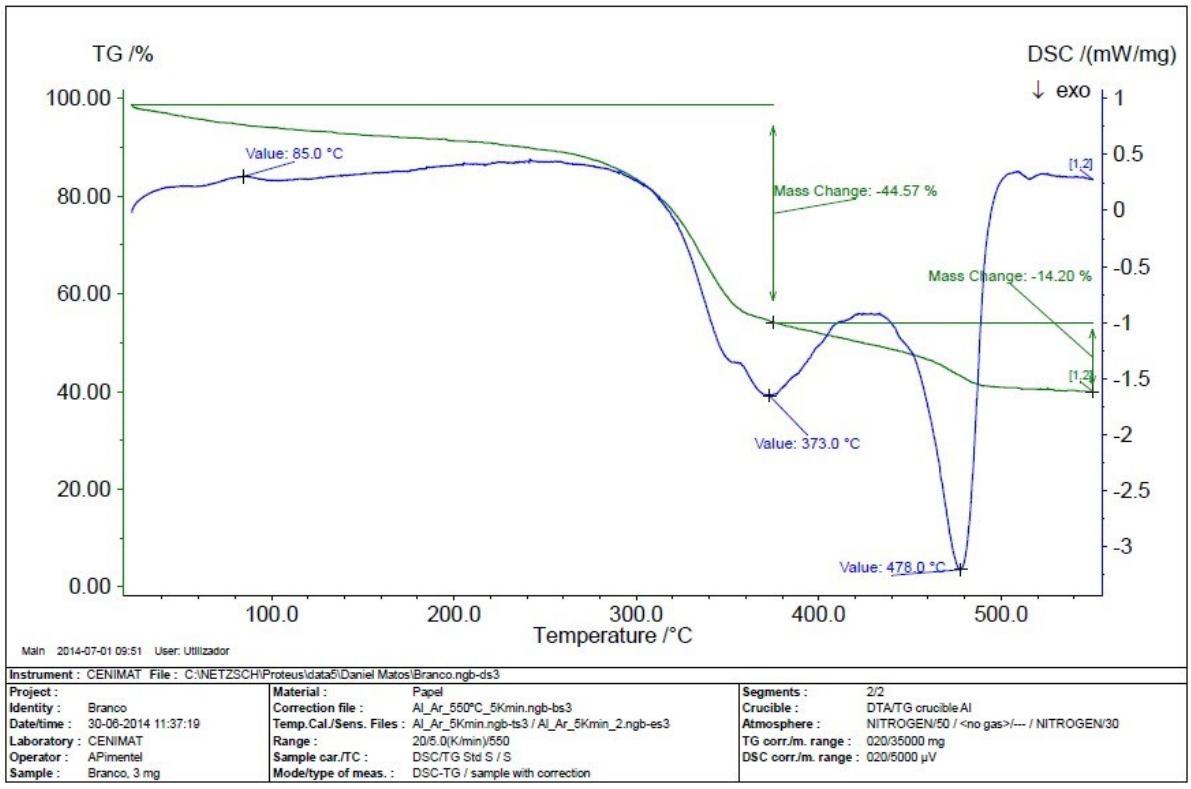

Figure 6.4 – DSC data of Lumi Paper

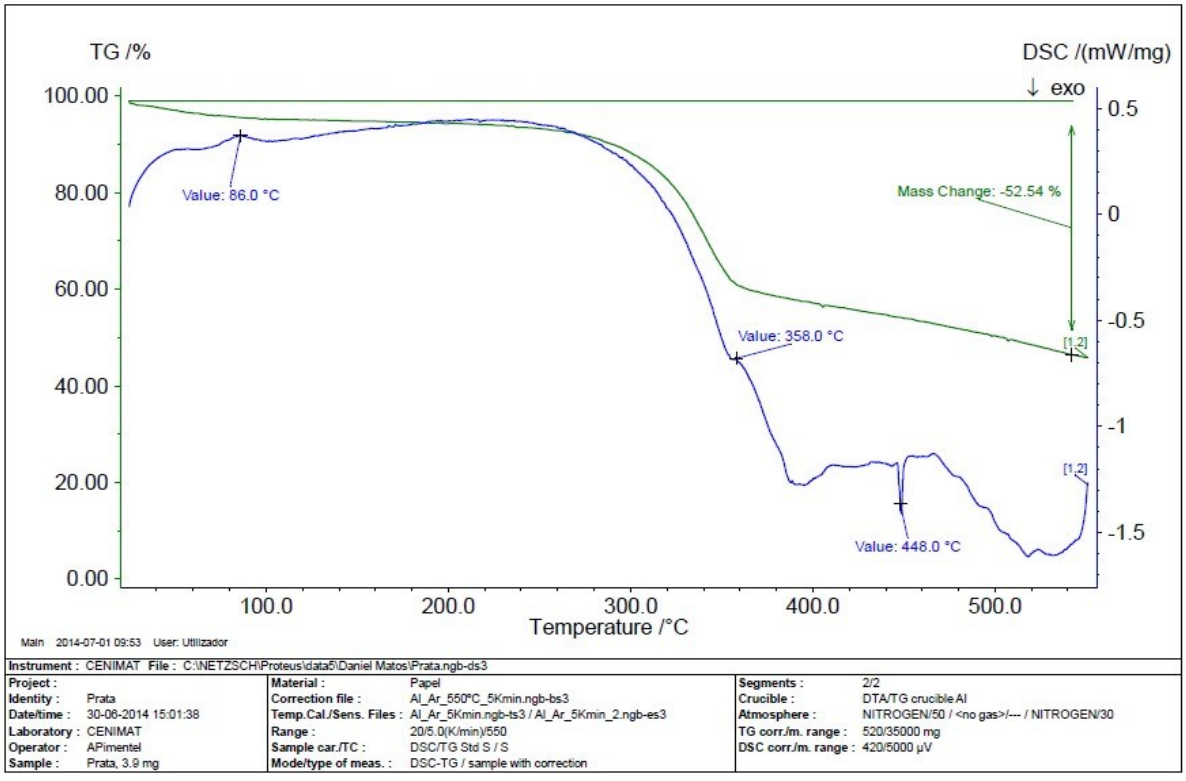

Figure 6.5 – DSC data of non-annealed silver on Lumi paper

Appendix E

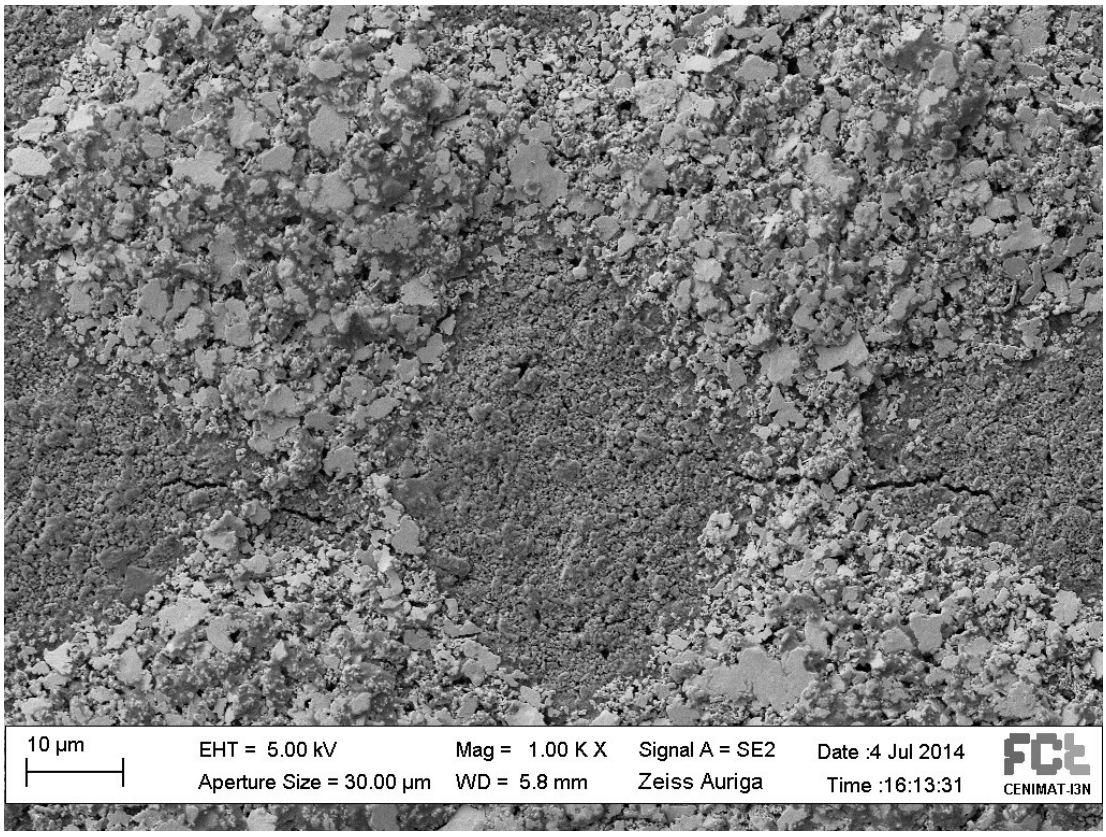

Figure 6.6 - Silver annealed in convection oven for 1 h at 100 °C

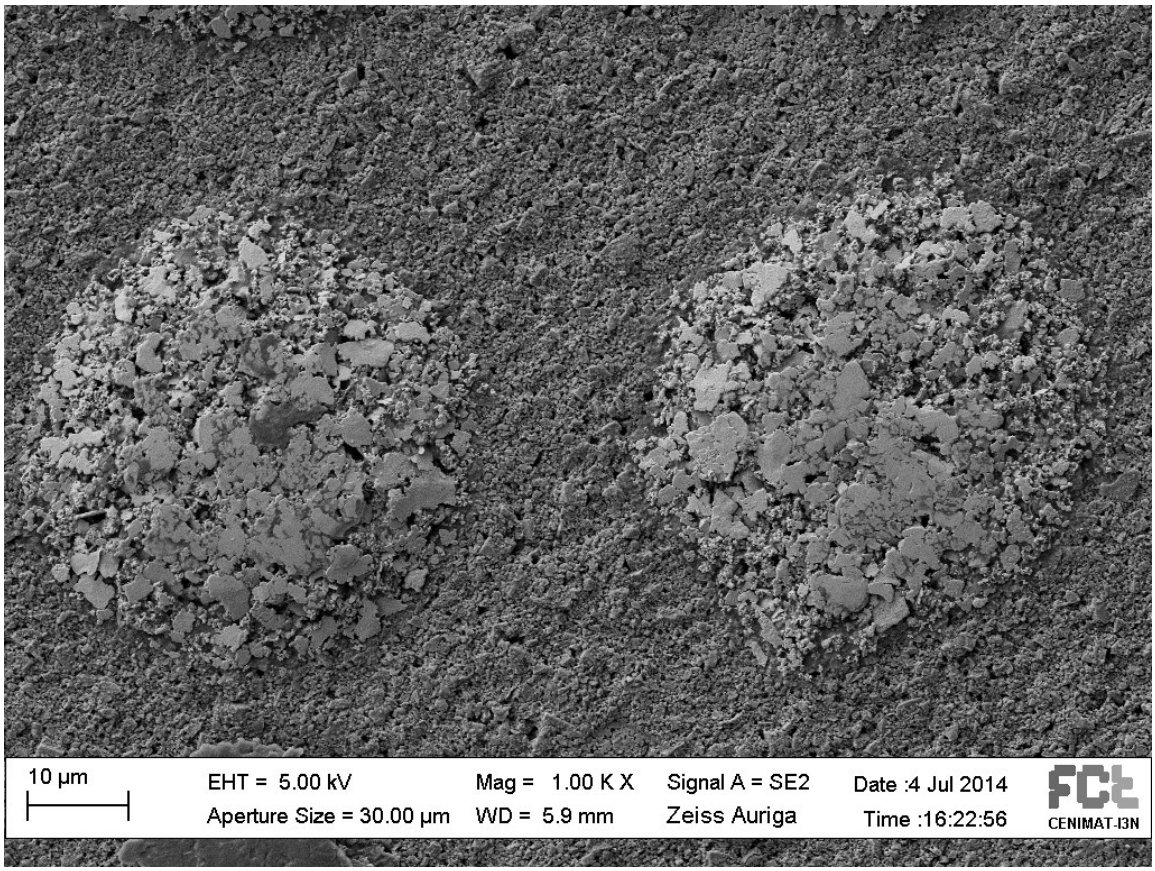

Figure 6.7 – Silver Silver annealed on hot plate for 10 min at 150 °C

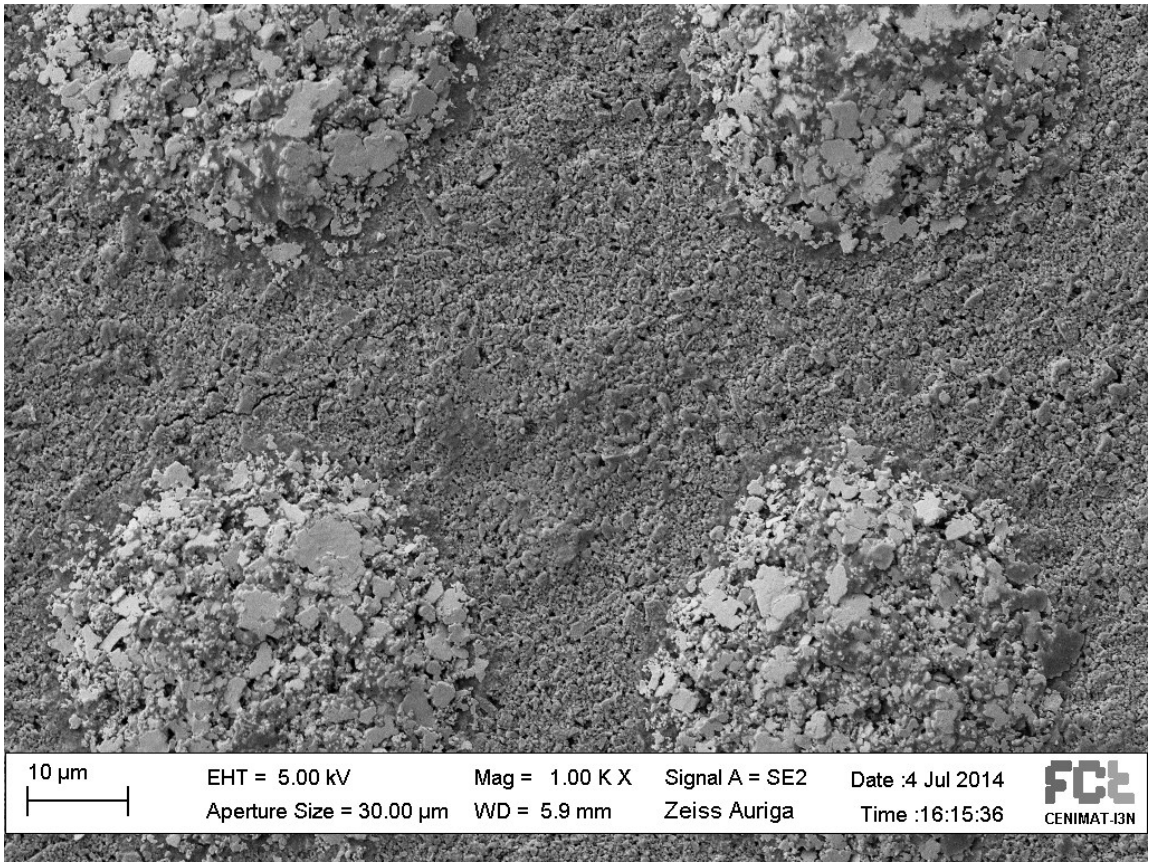

Figure 6.8 - Silver annealed in convection oven for 30 min at 100 °C

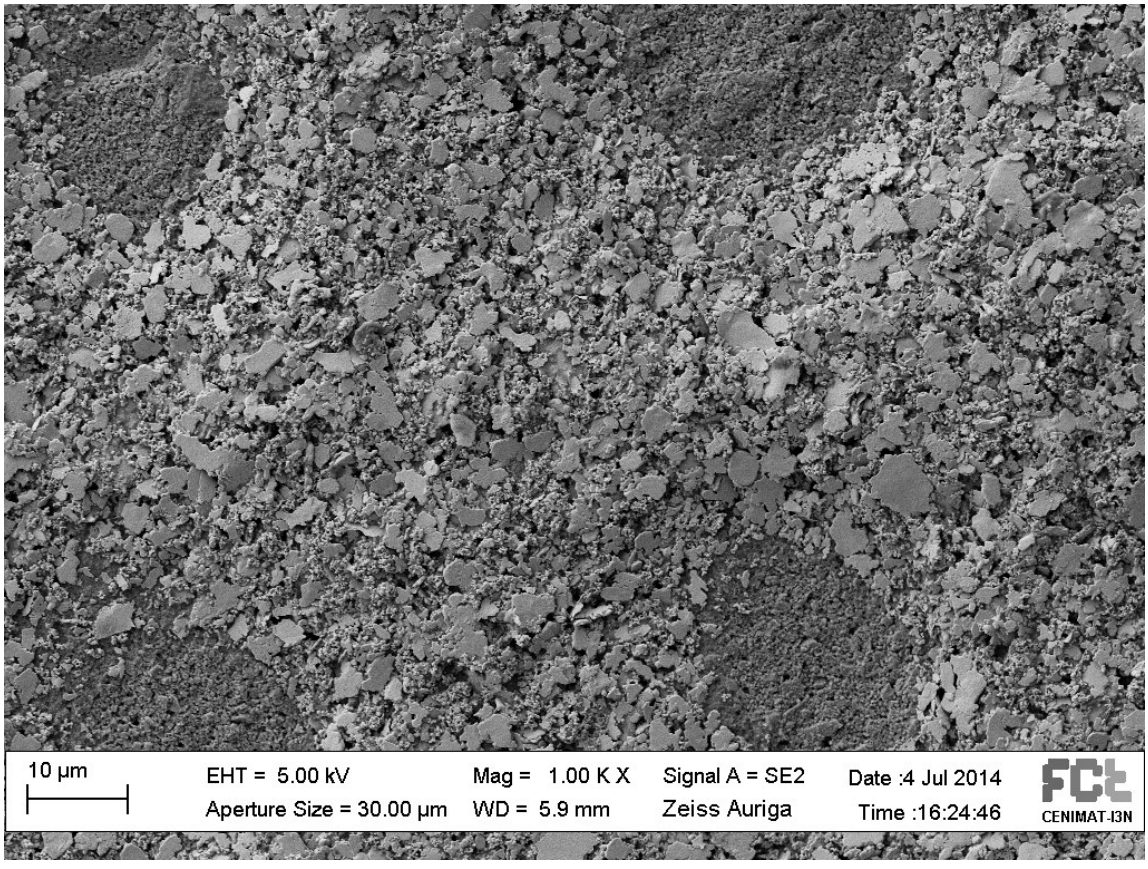

Figure 6.9 - Silver annealed in convection oven for 30 min at 150 °C

Appendix F

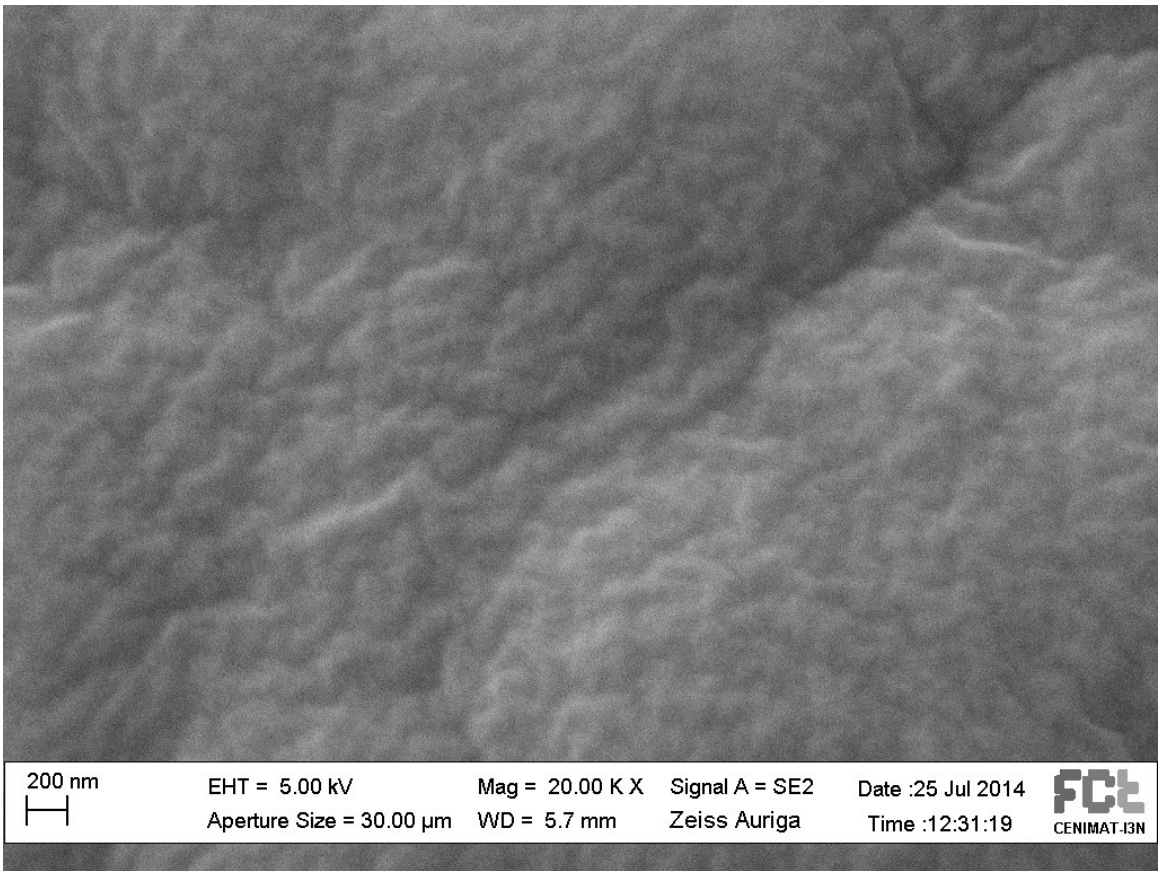

Figure 6.10 – Detail of the Parylene surface over Lumi paper.

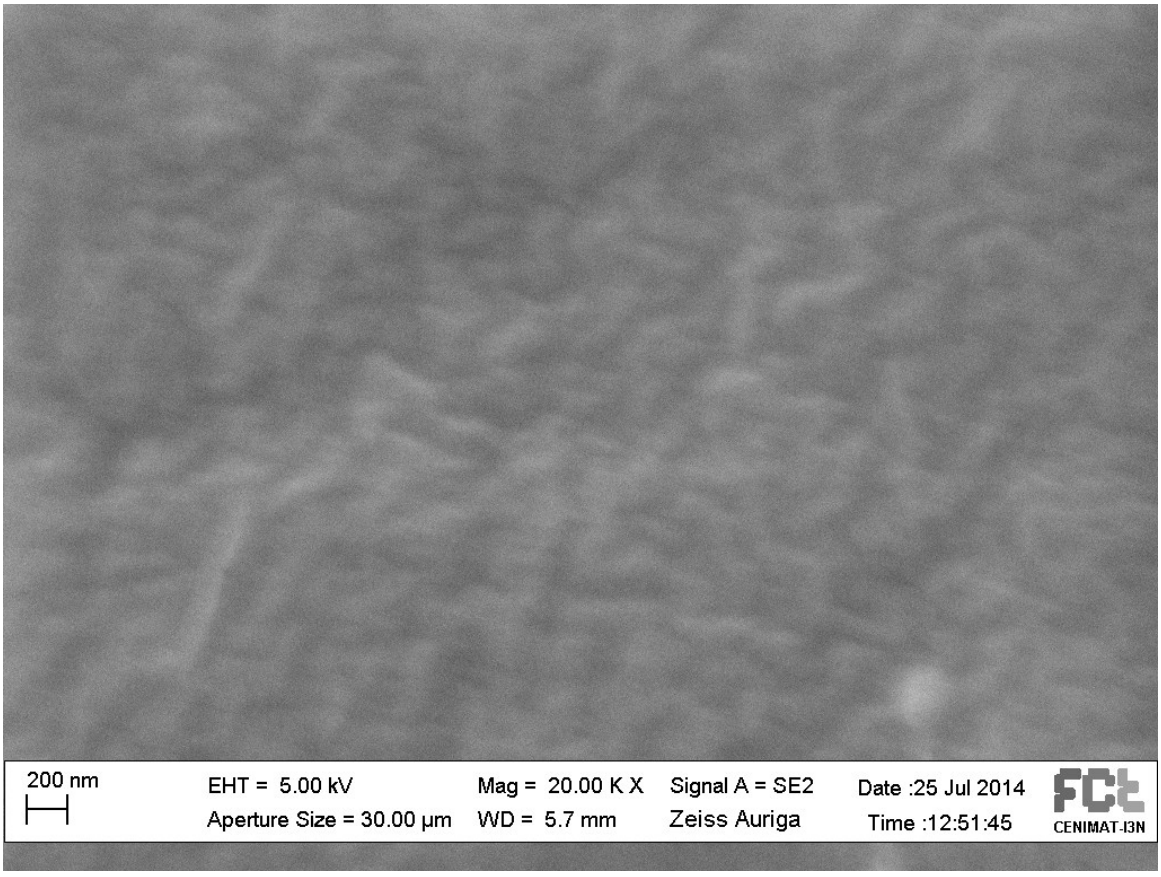

Figure 6.11 – Detail of the Parylene surface over Sappi paper.

Appendix G

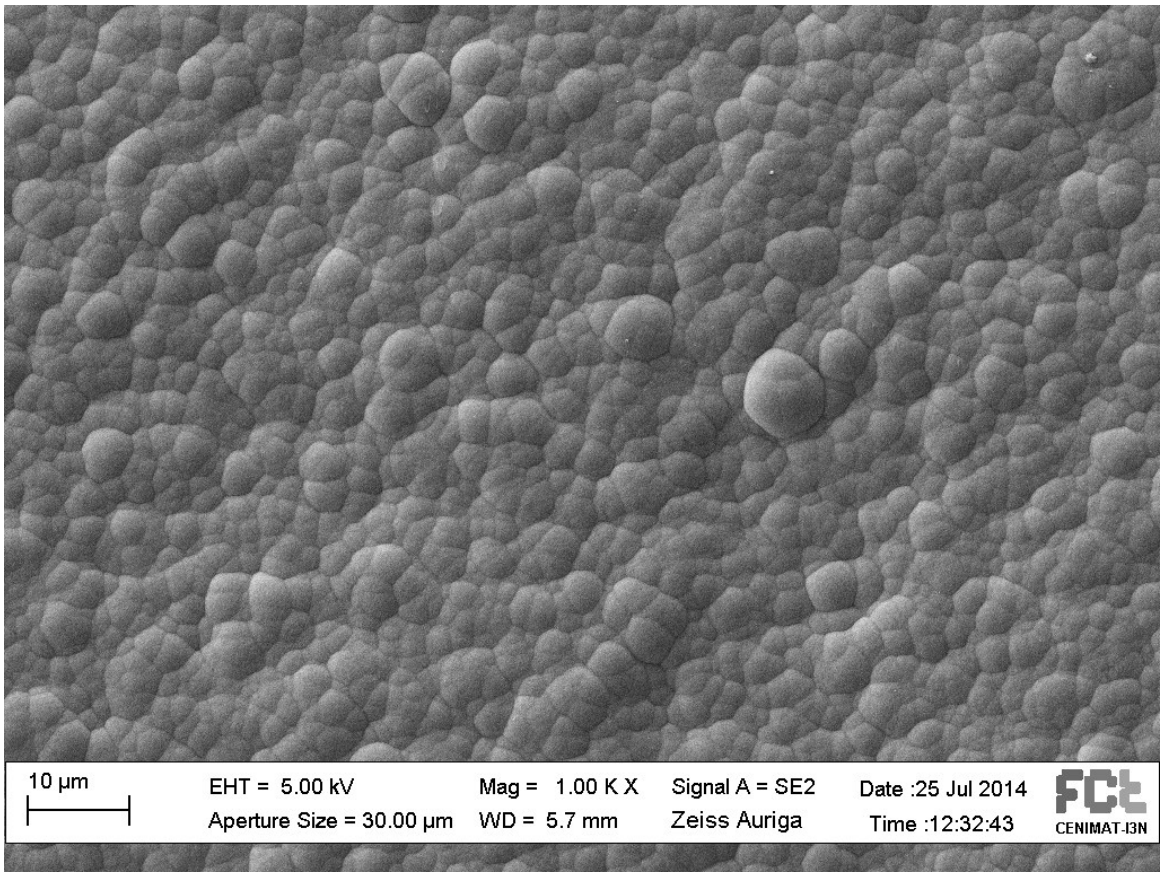

Figure 6.12 - Overview of the Parylene surface morphology over silver on Lumi paper.

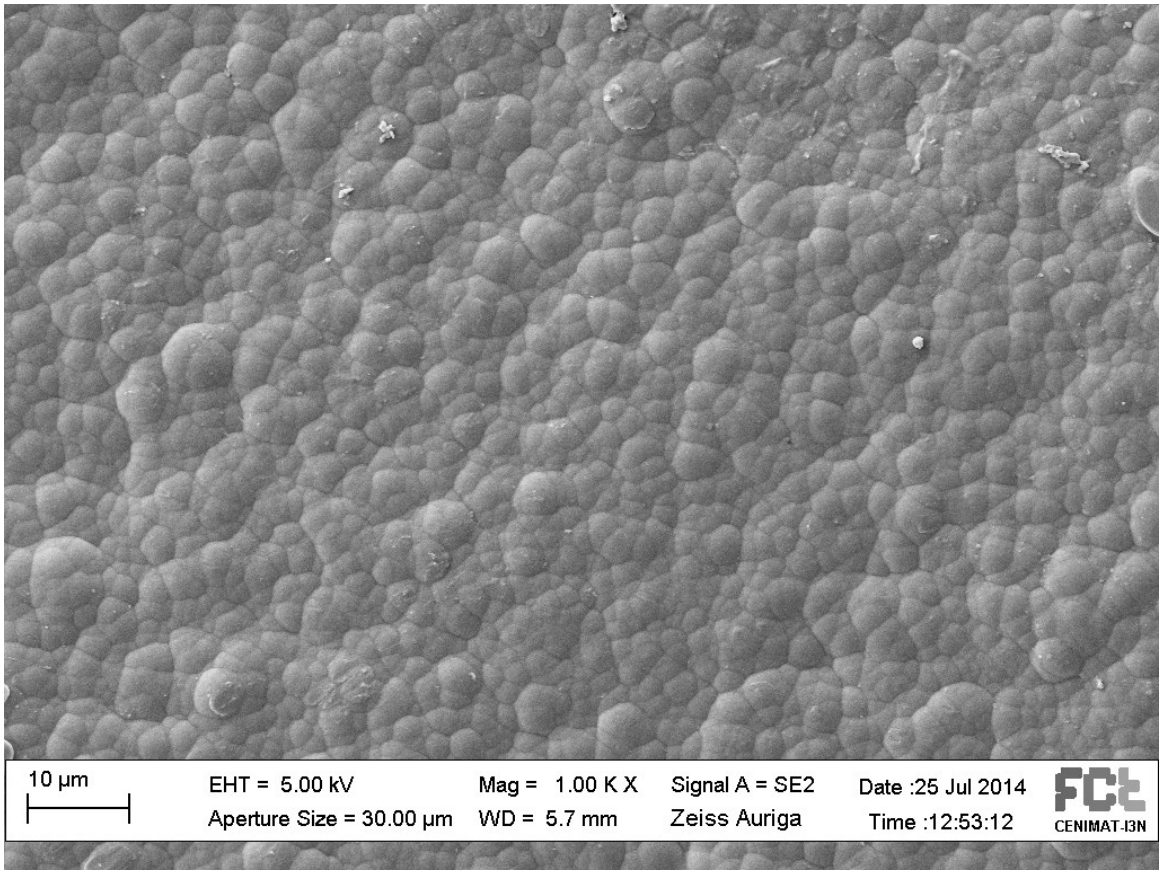

Figure 6.13 - Overview of the Parylene surface morphology over silver on Sappi paper.

Appendix H

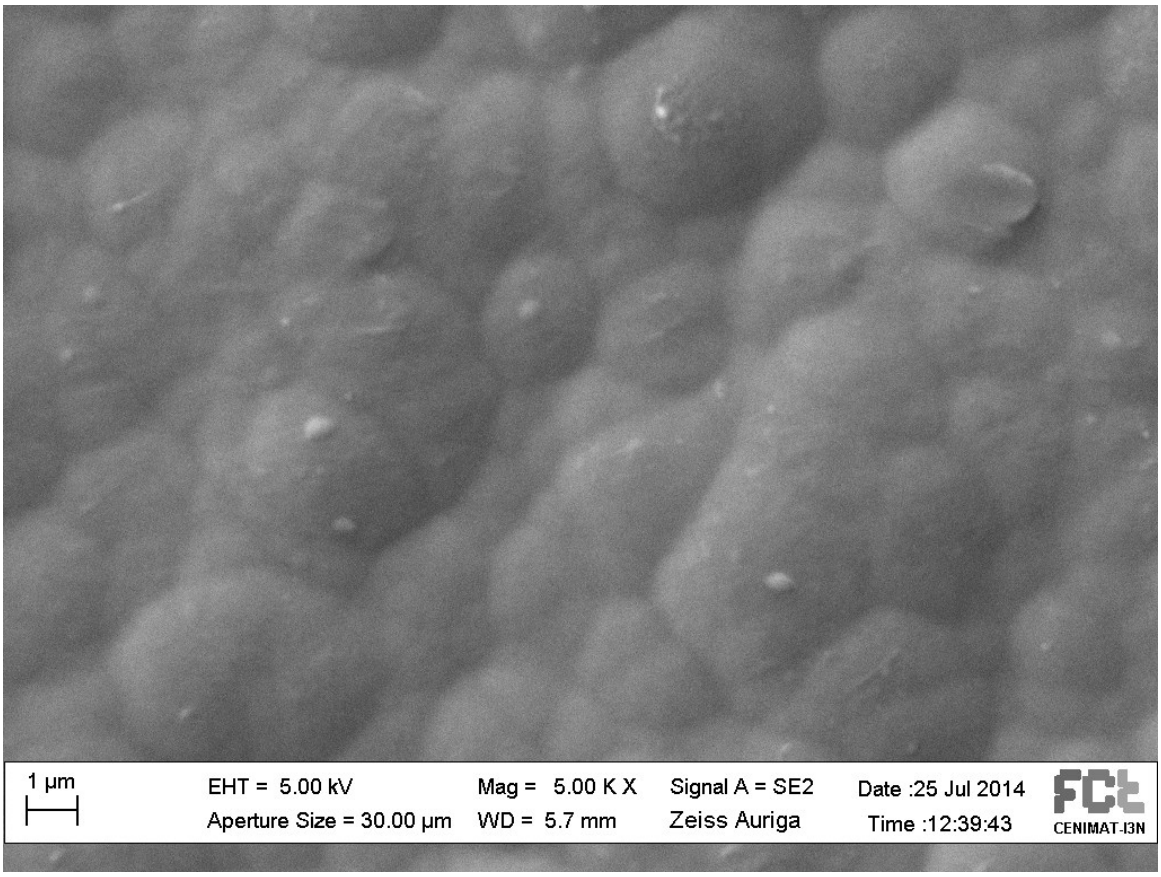

Figure 6.14 – Surface morphology of Teflon over Parylene directly over Lumi paper.

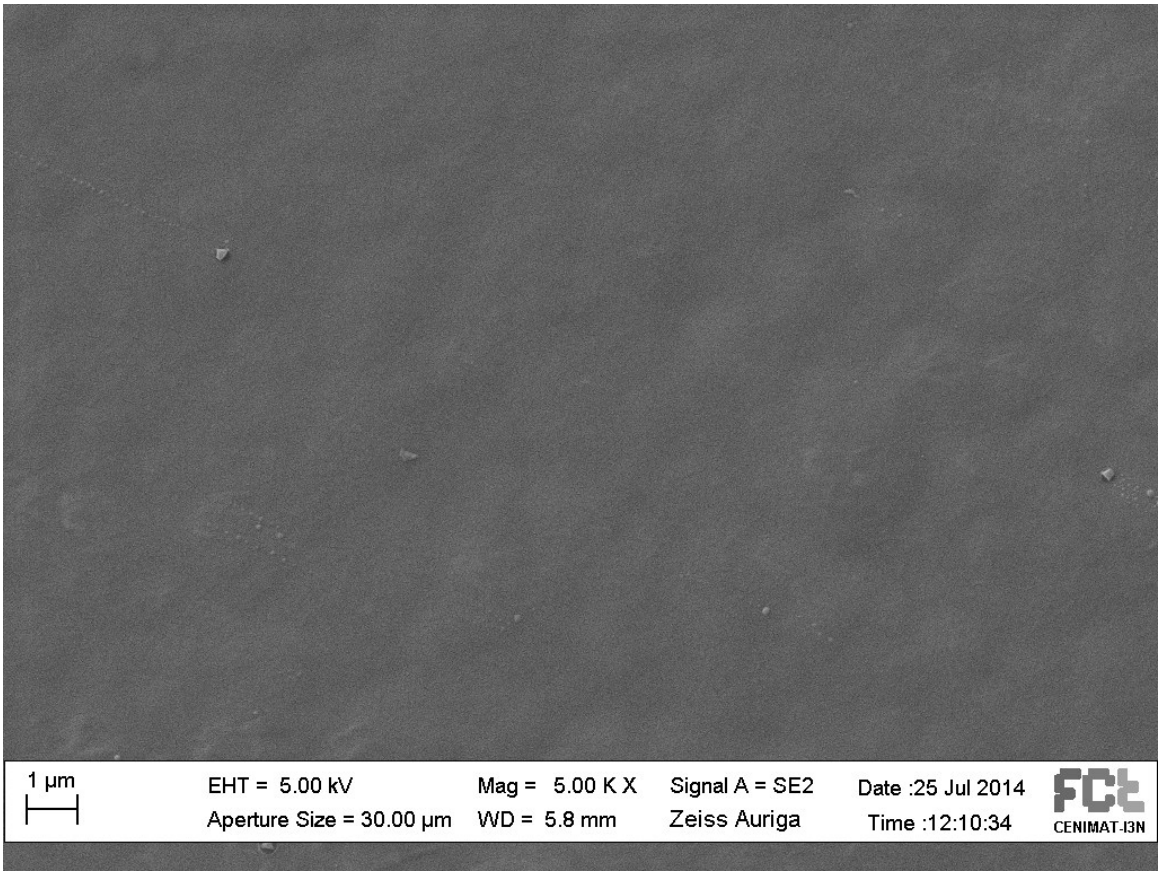

Figure 6.15 – Surface morphology of Teflon over Parylene directly over Sappi paper.

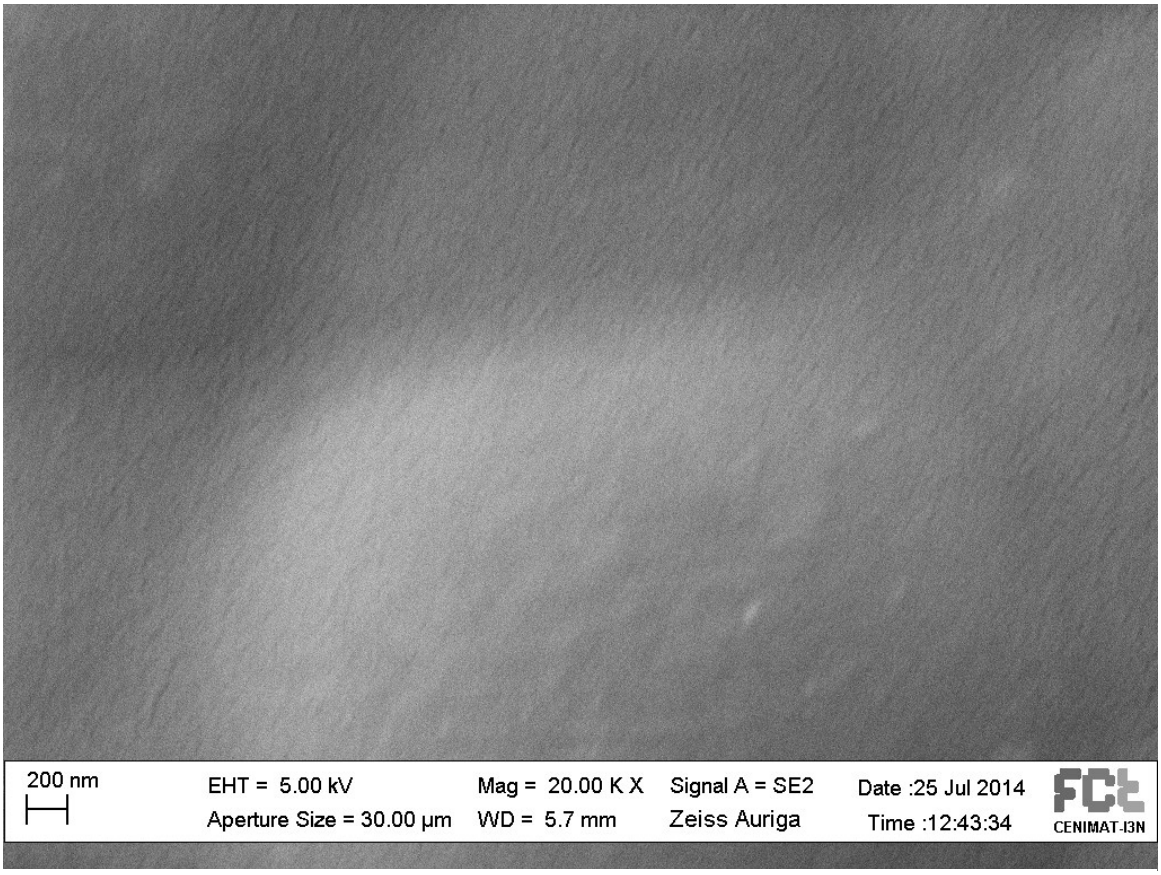

Figure 6.16 – Detail of Teflon surface over Parylene directly over Lumi paper.

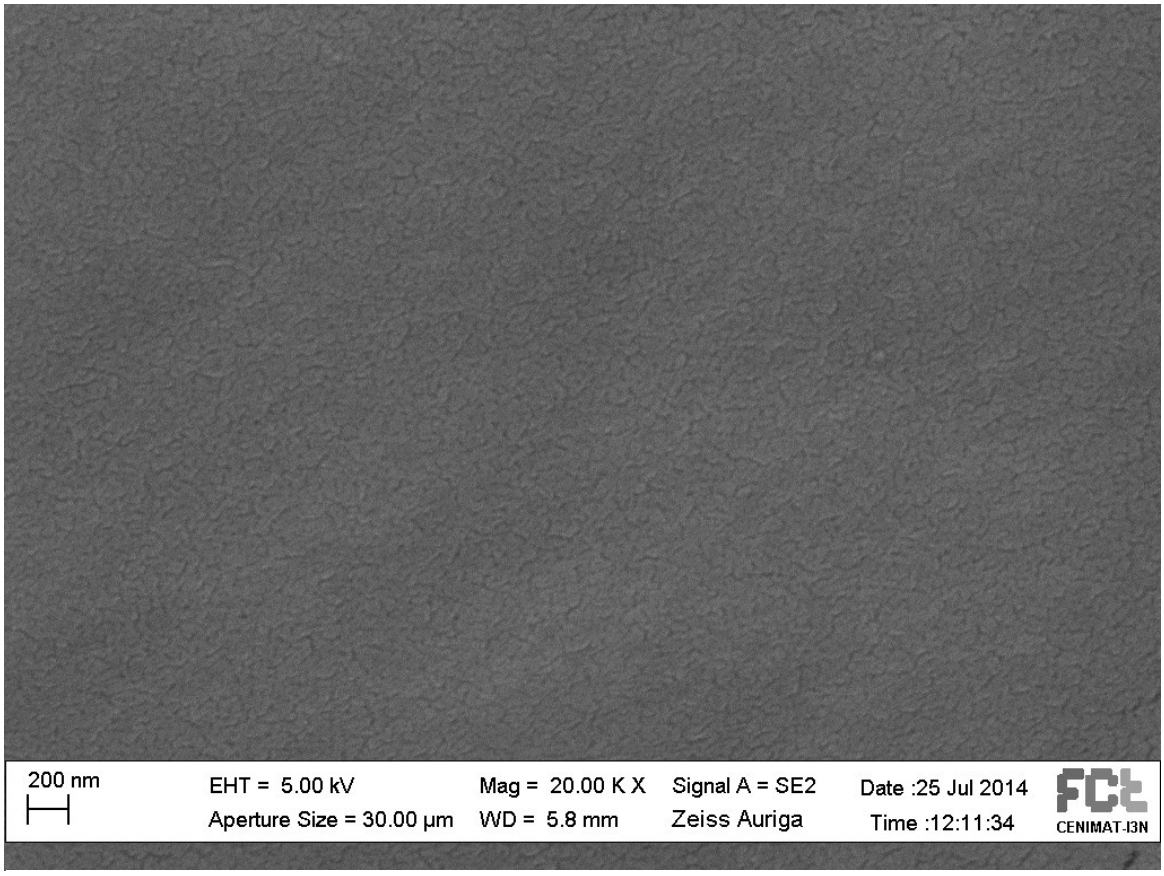

Figure 6.17 – Detail of Teflon surface over Parylene directly over Sappi paper.

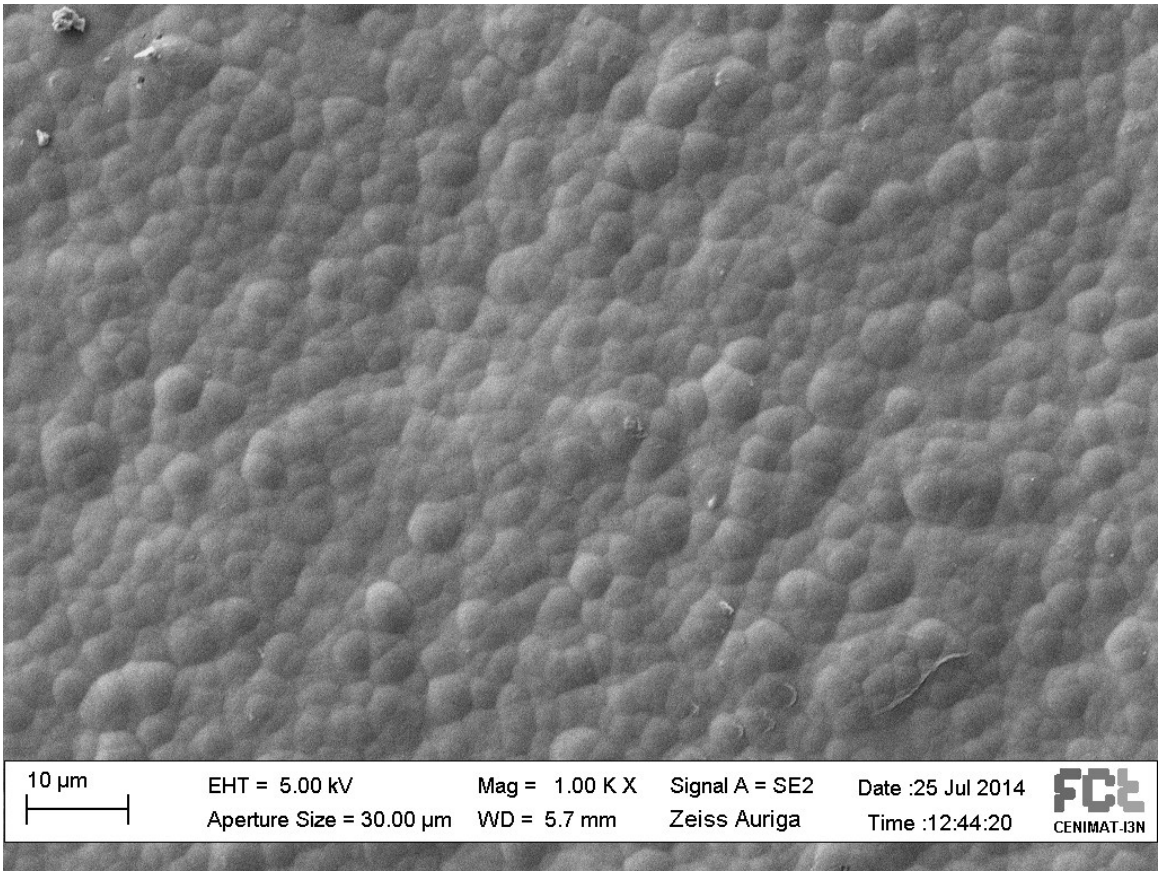

Figure 6.18 - Overview of the Teflon layer over Parylene on silver on Lumi paper.

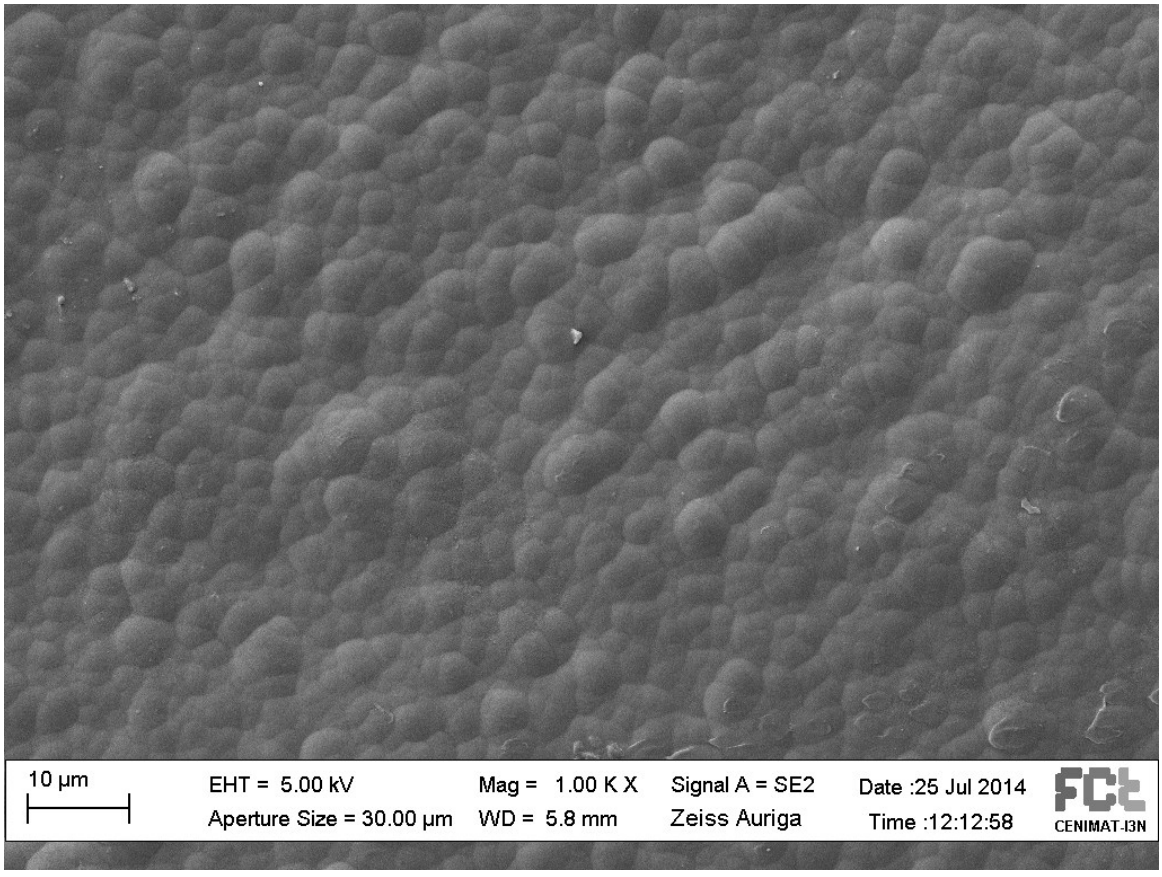

Figure 6.19 - Overview of the Teflon layer over Parylene on silver on Sappi paper.

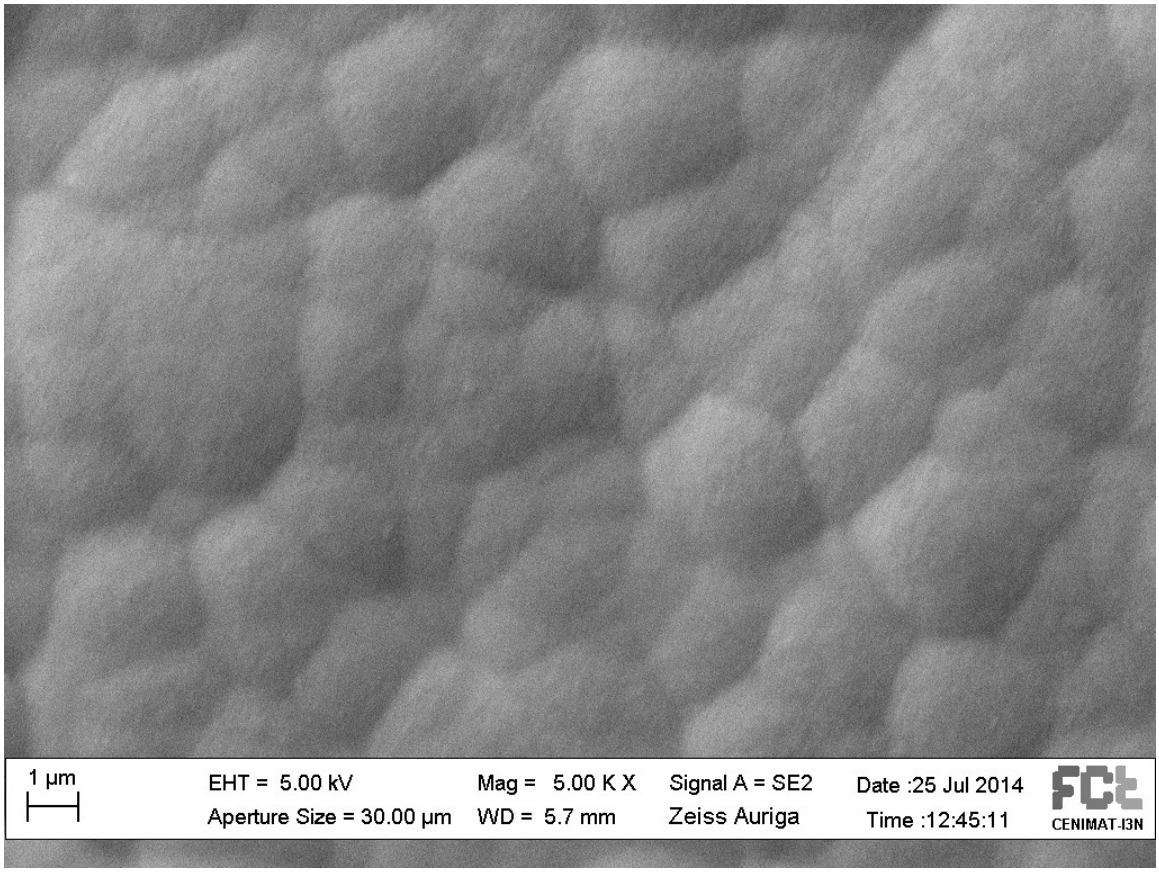

Figure 6.20 – Surface morphology with Teflon on Parylene silver on Lumi paper.

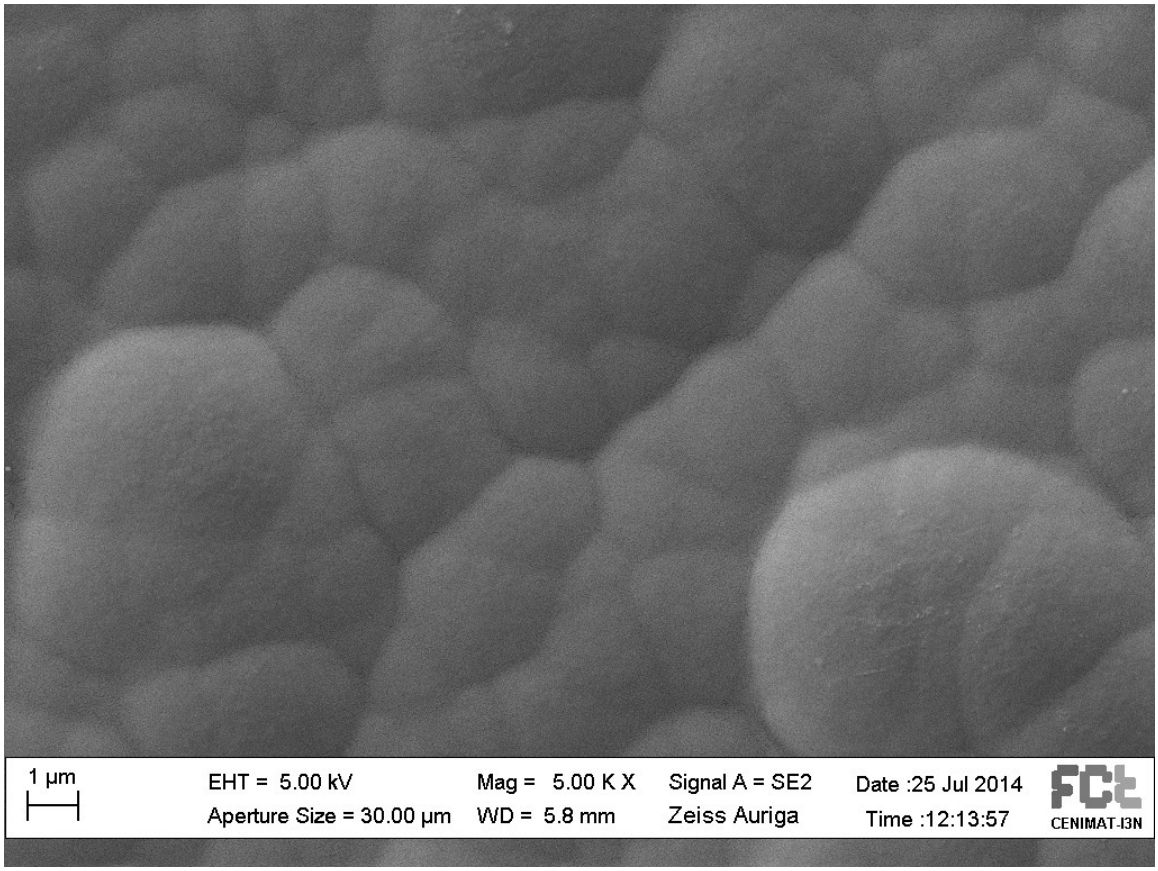

Figure 6.21 – Surface morphology with Teflon on Parylene silver on Sappi paper.

Appendix I

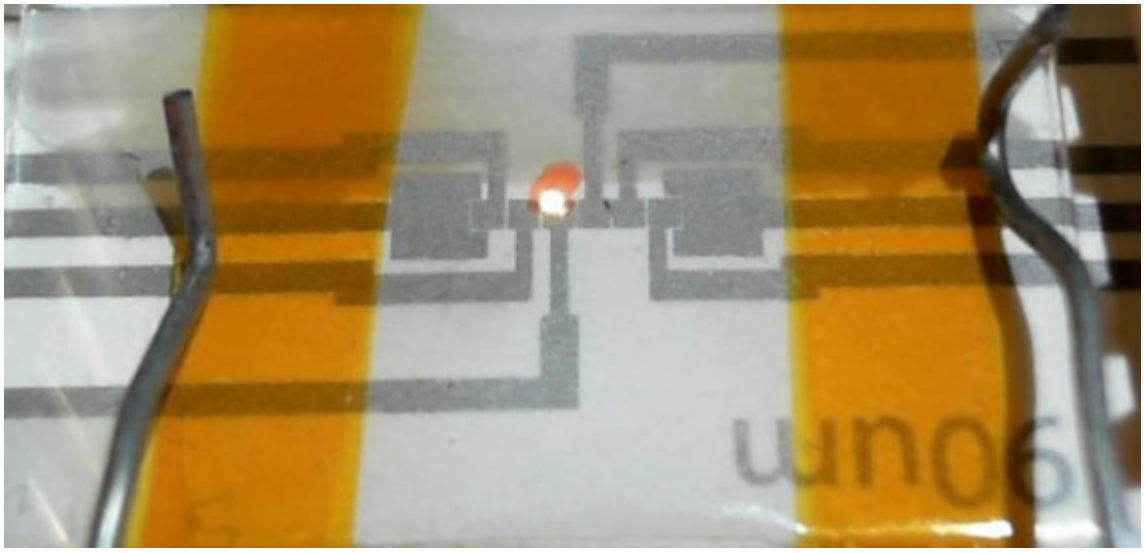

Figure 6.22 – Image of the breakdown during testing of a device with 2 µm Parylene thickness.

Appendix J

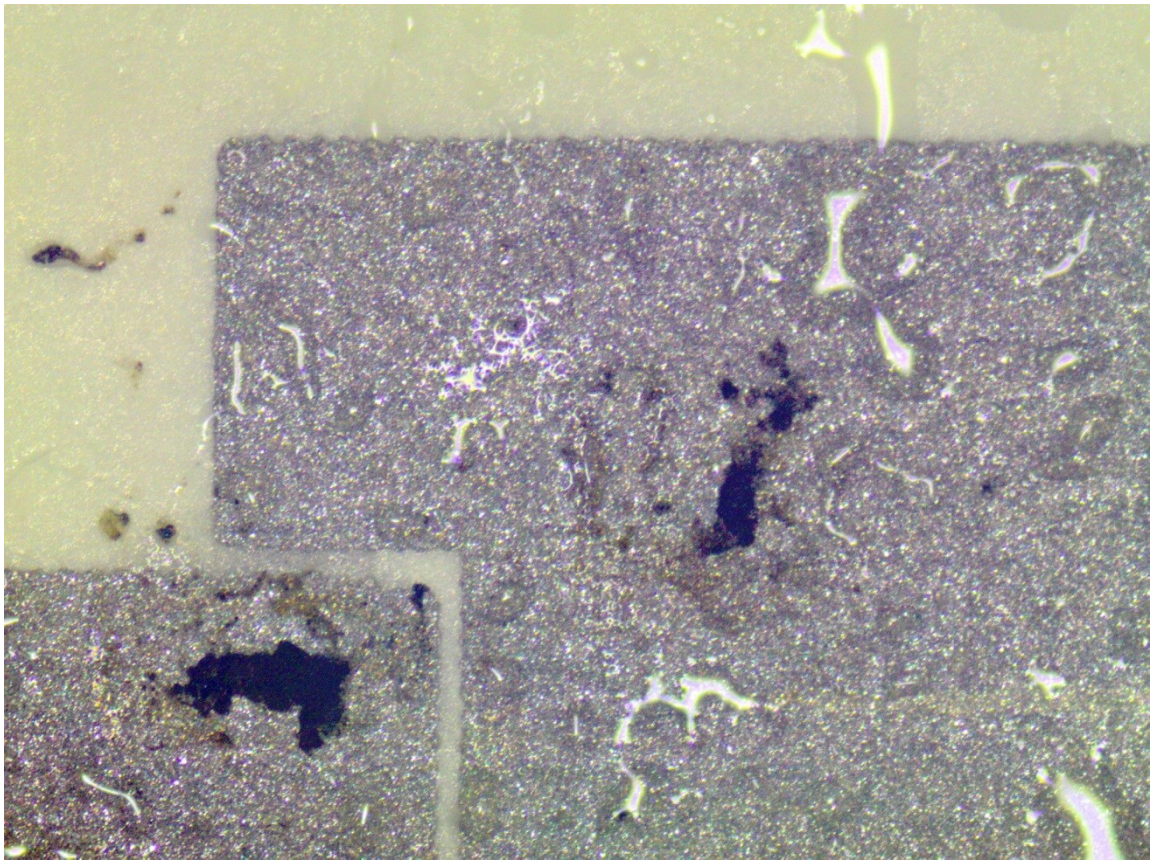

Figure 6.23 – Local results of the breakdown on a 2 µm Parylene thickness device.